Climate Dynamics (1997) 13:75–101

Climate Dynamics

Sensitivity of the ECMWF model northern winter climate to model formulation

Č. Branković, F. Molteni*

ECMWF, Shinfield Park, Reading, RG2 9AX, UK

Received: 30 November 1995 / Accepted: 13 July 1996

Abstract. The impact of various model formulations on model climate during boreal winter is studied using ensembles of seasonal integrations for four different versions of the ECMWF NWP model. The model versions, cycles 36, 46, 48 and 12r1, differ primarily in the representation of physical parametrization. In addition, higher vertical resolution was used for the 12r1 integrations. In the more recent cycles (48 and 12r1) a strong systematic overestimation of zonal flow over the northeastern Pacific has been dramatically reduced, contributing to a more realistic representation of the Pacific block. This improved representation of blocking, particularly in cycle 12r1, is linked to a more efficient diabatic response of the model to the warm SSTs in the western tropical Pacific. In contrast, over the Atlantic/European region a slight deterioration of blocking frequency in cycle 12r1 is associated with the strengthening of the Atlantic jet. The improvement in the Southern Hemisphere circulation, already evident in cycle 46, is not seen in the Northern Hemisphere, so it is argued that the impact of radiation changes introduced between cycle 36 and cycle 46 (inclusive) is influenced by seasonal cycle. A strong cooling of the southern (summer) polar stratosphere has been steadily reduced and in cycle 12r1 is about half of that seen in cycle 36. A reduction of errors in zonally averaged zonal wind and eddy kinetic energy is also clearly seen. In the tropics, the Hadley circulation has become more intense with the later cycles. This is associated with an intensification of convective rainfall within relatively narrow tropical convergence zones. Finally, it was found that the representation of interannual variations between strong positive and negative ENSO-index winters was most successful in cycle 12r1.

Correspondence to: Č. Branković, cbrankovic@ecmwf.int

**Present address:* Centro di Calcolo Interuniversitario dell'Italia Nord-Orientale (CINECA), Via Magnanelli 6/3, 40033 Casalecchio di Reno (Bologna), Italy

1 Introduction

A knowledge of the climate of a global numerical weather prediction (NWP) model or a general circulation model (GCM) is nowadays essential to assess the model's performance and its deficiencies. The model climate is normally derived from a number of relatively long, extended-range model integrations. The departure of the model climate from some observed or analyzed mean state of the atmosphere largely depends on the nature of the deficiencies in the model formulation. Systematic differences (errors) with respect to the real atmospheric state may also be influenced by "external" factors, such as the way the lower boundary forcing is formulated. However, we consider here only the errors induced by deficiencies intrinsic to the model. In short- or medium-range forecasts, model systematic errors may not always manifest themselves strongly enough to be detectable with high statistical significance; therefore the study of model errors on longer time scales may help to better define and understand the systematic effects of errors in model formulation, and eventually lead to their correction. On the other hand, relatively strong systematic errors in the short or medium-range period may be due to a relatively fast "adjustment" of the model atmosphere, and a simple extrapolation of these errors in time may not necessarily lead to an appropriate estimate of the equilibrium model climate. Figure 2 in Palmer et al. (1990) demonstrates this "two-way" relationship between medium-range systematic errors and "long-term" errors from a relatively large set of European Centre for Medium-Range Weather Forecasts (ECMWF) monthly forecasts.

In the continual effort to improve the accuracy of NWP, it is necessary to modify frequently the formulation of a numerical model in order to introduce more efficient numerical schemes and more accurate or detailed parametrizations of physical processes. Changes to the model formulation necessarily influence systematic errors and ultimately model climate. Scientific literature discussing causal relationships between climatologies of various models and their formulation is

abundant. Various aspects of model numerics, horizontal and vertical resolutions, physical parametrization or representation of orography, are usually addressed (see, for example, WMO 1988; WMO 1991; Le Treut 1996). In the past decade or so a number of studies comparing a specific modelling aspect in *different* models has been increased. For example, Slingo et al. (1996) studied intraseasonal oscillation in 15 atmospheric GCMs from the Atmospheric Model Intercomparison Project (AMIP). The main objective of these studies is to try to identify deficiencies common to many models and to possibly formulate hypotheses about the causes of such deficiencies.

Relatively few studies deal with evolutionary improvements in model climates. Sirutis and Miyakoda (1990) discussed the impact of the four different subgrid scale parametrization packages on January integrations of the GFDL model. The four model versions were formulated by accumulatively increasing the elaboration and the sophistication of the physics. The superiority of the more complex version of the model physics is evident in the last 10 days of the one-month forecasts. Hurrell (1995) comprehensively documented model climates and biases of the four versions of the widely used NCAR Community Climate Models (CCMs). The models were integrated for 10 years at relatively low horizontal resolution. Overall, the CCM2 version, which included more recent developments in physical parametrization and semi-Lagrangian transport scheme for advecting water vapour, seems to be superior to the other models.

In this study we assess various aspects of the impact of some modifications to the formulation of the ECMWF NWP model on the model climate during the northern winter. Four versions of the ECMWF operational model were studied. These model versions are denoted as model cycles 36, 46, 48 and 12r1 with cycle 12r1 being the latest. For each cycle of the model, the model climate was derived from seasonal integrations in a consistent fashion. Our study was, to a certain extent, constrained by ECMWF operational requirements and, as noted by Hurrell (1995), diagnosing a straightforward relationship between model errors and specific change(s) in model formulation may be difficult without conducting carefully planned sensitivity experiments.

In the following section a brief summary of meteorological changes introduced with model cycles 36, 46, 48 and 12r1 is given. In Sect. 3 the organisation of experiments used in estimating the model climate is described. Section 4 deals with upper-air wintertime circulation, mainly in terms of errors and differences among the four model cycles. The blocking frequency and circulation regime statistics are given in Sect. 5. The impact of model changes on precipitation is discussed in Sect. 6. In Sect. 7 some aspects of the simulation of interannual variations are shown. Section 8 concludes the work with a summary and discussion of our results.

2 Summary of changes to model formulation

Detailed descriptions of various numerical, physical and technical changes to the ECMWF model formulation are found in relevant ECMWF Research Department documentation. We summarize the model changes introduced with model cycles 36, 46, 48 and 12r1. Some emphasis on the most important changes is given, and the motivation for implementing them in the model is briefly discussed. Other changes to both physical and dynamical ECMWF model formulations were also introduced over the period since cycle 36 came into operations; the principal changes are listed in Table 1. Many of them were mainly of technical nature, and some, as for example the semi-Lagrangian dynamics and related modifications, are not relevant for this study as all runs are at T63 resolution and use an Eulerian time scheme (see the next section on organization of experiments).

2.1 Cycle 36

Cycle 36 of the model (hereafter referred as CY36) was introduced in operations on 5 June 1990 and included several changes (see ECMWF Research Department Memos R2314/2618 and R2314/2617). This model cycle was used for much of ECMWF experimentation on the seasonal time scale. A detailed description of the CY36 climatology is given in Ferranti et al. (1994a), and extended range predictability using 3-member and 9-member ensembles respectively was discussed by Branković et al. (1994) and Branković and Palmer (1996).

Parametrization of surface fluxes at low wind speed over the sea

From preliminary experimentation with enhanced SSTs in the western Pacific and Indonesian region, a remarkable model sensitivity was found. Such a forcing was applied in the warm pool region, where wind speeds are relatively low; further experiments confirmed that the model was deficient in parametrizing evaporation at low wind speeds. The formulation of the transfer coefficient for moisture between the surface and the lowest model level has been improved and consequently the latent heat flux was increased. With this modification, a more realistic rainfall pattern in the tropics was produced and easterly wind error was reduced (Miller et al. 1992).

Radiative effects of non-precipitating convective clouds

Before CY36, the convective cloud cover was dependent on time-averaged precipitation rate, and non-precipitating convective clouds (like trade wind cumuli and fair weather cumuli) were not represented in the radiation calculation. The convective cloud formulation was therefore modified to use a dependency on the condensation rate rather than the precipitation rate. The

Table 1. Principal changes to the model formulation from cycle 36 to cycle 12r1

Model cycle	Date	Modifications
36	**5 Jun 1990**	**Surface fluxes for low wind speed over sea** **Convective cloud formulation** **Implicit gravity wave drag introduced**
37	12 Feb 1991	Technical changes
38	9 Apr 1991	Maximum overlap of cloud layers Cooling to space above 10 mb Vertical diffusion above PBL Revised convection
39	17 Sep 1991	Semi-Lagrangian scheme, reduced grid, T213 model, 31 levels New horizontal diffusion (T213 only) Cloud scheme modified Timestep-dependent convective mass flux limit Partially implicit normal mode initialization
40	26 Nov 1991	Corrected bug in longwave radiation
41	7 Jan 1992	Horizontal diffusion modified (T213 only) Time-stepping algorithm for cumulus momentum transfer changed
42	13 May 1992	Mass flux limit in convective parametrization corrected Treat sea ice as land in free convective regime Virtual temperature as spectral variable Optimized semi-Lagarangian trajectory calculations, optimized radiation
43	17 Aug 1992	Vertically non-interpolating semi-Lagrangian scheme, smaller time filter Explicit time scheme for cumulus momentum transfer Changes to sea ice parametrization Modified treatment of low-level inversion clouds Consistent interpolation between full and half level temperatures in radiation
44	1 Sep 1992	Technical changes
45	7 Dec 1992	Technical changes
46	**1 Feb 1993**	**Include shortwave optical properties for ice and mixed phase clouds** **Revise clear sky absorption** **Pure del 4 horizontal diffusion (T213 only)**
47	21 Apr 1993	Technical changes
48	**4 Aug 1993**	**Entrainment at top of PBL** **Increased entrainment in shallow convection** **Modified roughness length and air-sea transfer coefficients** **New parametrization of soil processes**
49	5 Oct 1993	Changes to skin and 2 m temperature profile function
11r7	**2 Mar 1994**	**New closure in shallow convection** **Inclusion of latent heat release due to freezing of condensate in convective updrafts** **Distinction between water and ice clouds in radiation scheme changed**
12r1	23 Aug 1994	Technical changes

effect of the change is an increase of the total cloud cover, enhancement of evaporation over subtropical oceans and a reduction of precipitation over the continents.

The third modification in CY36 was the introduction of an implicit formulation of gravity-wave drag parametrization; this model modification had negligible meteorological impact.

2.2 Cycle 46

Cycle 46 (CY46) was introduced in operations on 1 February 1993 (see ECMWF Research Department Memos R60.6.1/4/PA, R60.6.1/5/PA and R60.6.1/AS/302). The main modifications were introduced to the cloud and radiation parametrization (Morcrette 1993). Also, the horizontal diffusion was modified, but this is relevant only for the operational (T213) resolution of the model.

Revision of the cloud radiative properties

The diagnostics of the model performance indicated an excessive radiative cooling below the tropopause at high-latitudes, with clouds playing an important role in this cooling. In addition, the heating over the continents in summer was found to be overestimated. In the new formulation, the scattering properties for ice clouds were introduced in terms of the ice water path. Modified shortwave cloud properties increased heating by absorption of solar radiation in the higher level clouds (where the ice fraction is dominant) and decreased downward solar radiation below these clouds. The reduction of the net radiative cooling in the high clouds was particularly evident in summer hemispheres.

Revision of the clear-sky absorption coefficients

An outdated definition of absorption coefficients for the radiation scheme was replaced by a new one, based on a more recent spectroscopic data. Also, the longwave and shortwave radiative effects of a climatological distribution of aerosols were revised. All these changes led to an overall increase in the atmospheric

shortwave absorption and a decrease in downward shortwave radiation at the surface.

2.3 Cycle 48

Cycle 48 (CY48) was introduced in operations on 4 August 1993 and included four changes to the parametrization of surface and planetary boundary layer (PBL) processes (see ECMWF Research Department Memo R60.6.1/145/PA). Some of the pre-CY48 model deficiencies related to those processes could be summarized as the following: the total heat flux was too large over land surfaces with a large phase error in the diurnal cycle, the boundary layer depth was too shallow and too moist indicating a lack of boundary layer entrainment, soil moisture was strongly influenced by the model climate layer, evaporation from the surface was too large in wet conditions, and the runoff amounts were relatively large even when the soil was dry. The CY48 changes have been also discussed by Beljaars et al. (1996).

Enhancements to the parametrization of the soil processes and skin layer temperature

The new soil scheme has four prognostic layers for soil moisture and soil temperature (Viterbo and Beljaars 1995). The hydrologic diffusivity and conductivity are defined as non-linear functions of the soil moisture, and the runoff is mainly due to the gravitational drainage. The skin layer with no heat capacity was introduced in order to have a faster adjustment of the sensible and latent heat fluxes to the radiative forcing. Separate roughness lengths for momentum and heat were assumed. With the new scheme, the evaporation is maintained for longer periods and the soil dries out less quickly.

Introduction of entrainment at the top of the PBL

In the unstable regime, an entrainment parametrization was introduced by specifying the diffusion coefficient in the capping inversion so that the buoyancy flux in the entrainment layer is proportional to the surface buoyancy flux. In the stable regime, the old scheme is used but with less diffusion at large Richardson numbers. (The old scheme was based on stability-dependent exchange coefficients as a function of the Richardson number below the inversion, and on Monin-Obukhov formulation above the PBL height.) These changes have an overall effect in increasing the depth of the PBL.

Other changes

Two additional changes have been also introduced: entrainment in shallow clouds was increased and roughness length together with air-sea transfer coefficients were modified. For a discussion on the latter modification see Beljaars (1995). The shallow convection change makes the convection less deep and enhances the mixing across the inversion thus moistening the levels around 850 mb.

The multi-year integration with CY48 changes yielded more realistic annual cycle of soil moisture and soil temperature with decreasing amplitude with depth and a correct phase lag. Also, a general reduction of the model systematic errors, mainly in the tropics, was seen.

2.4 Cycle 12r1

Although cycle 12r1 was introduced in operations on 23 August 1994, it represented per se only some minor technical modifications to the previous cycle (11r7) which had been in operations since 2 March 1994 (see ECMWF Research Department Memo R60.6.1/21/PA).

Changes to the convection scheme

For the closure of the shallow convection scheme, the sensible heat flux is taken into account in addition to the latent heat flux. This modification caused an enhancement in the convective activity resulting in an increase in the tropical specific humidity.

The second change was a correction of the latent heat release due to freezing of condensate in the convective updrafts together with a simple mixed-phase partitioning depending on temperature. In addition, the distinction between water and ice clouds in the radiation scheme was changed to be consistent with the distinction in the convection scheme. The effect of these modifications was a weak warming of the model atmosphere.

In addition to the modifications in the model physics, our experiments with cycle 12r1 also included 31 levels in the vertical (see next Sect.). However, this 31-level model and all earlier model cycles studied here, which were run with 19-levels, extended in the vertical to the same height in the stratosphere, up to 10 mb. With 31 levels an approximate doubling of vertical resolution between the boundary layer and stratospheric model levels was achieved. It is important to emphasize that such an increased vertical resolution in the model certainly contributed to the changes in the model climate. However, based on the experience with further ECMWF experimentation, we assume that the impact of model physics modifications introduced with cycle 12r1 is dominant over that due to increased vertical resolution. Cases when this assumption is not appropriate will be explicitly discussed.

3 Experiment design

The experiments reported here with CY36, CY46 and CY48 were run at T63L19 model resolution. For cycle

12r1 there were 31 levels in the vertical, i.e. the model used was T63L31. (It has to be noted that 31 levels were introduced in the ECMWF operational model with model cycle 39, see Table 1.) The length of simulations was approximately 120 days, depending on initial date. The experimentation covers five winter seasons (DJF), from 1986/87 to 1990/91. For each winter three integrations initiated on the same calendar dates, 1, 2 and 3 November, were carried out. All experiments were run with Eulerian dynamics and on a full model grid.

In the runs with CY36, CY46 and CY48, the observed sea surface temperature (SST) was updated every 5 days throughout the integration. In 12r1 on the other hand, the SST boundary forcing was updated in the model daily by interpolating from monthly average SSTs. It is assumed that this relatively small inconsistency in the SST forcing in 12r1 has less important impact on seasonal time scale integrations compared to the impact arising from the changes to the model formulation.

For each model cycle considered, the model climate was computed from the average of all 15 experiments. Only the last three months, corresponding to the conventional winter calendar season, were analyzed. The ensemble (seasonal) averages were computed from seasonal averages of respective individual experiments. For verification purposes the (ensemble) seasonal averages from the 5-winter ECMWF analyses were also calculated. Such a verification may be more "biased" towards earlier model cycles, in particular in data sparse regions, since the analyses were made with an earlier and therefore more similar version of the model (see also discussion in Sect. 4.5).

The changes to the parametrization of soil processes in CY48 made obsolete the use of deep climatological soil-moisture and soil-temperature fields. However, no re-assimilation for the initial data has been done; the initial data for CY48 and 12r1 were obtained from operationally archived data using standard ECMWF procedures.

Since the size of our ensembles may suggest sampling inadequacy, for each model cycle we computed a t-statistic to test the significance of the mean difference between 15 model runs and 5 winter analyses. The t-statistic determines the statistical significance of the model error, i.e. it indicates how *systematic* is the mean error computed from a limited sample. In particular, the spatial distribution of t-values clearly indicates the regions where the impact of model deficiencies is larger than sampling errors associated with the internal variability of the atmosphere. When evaluating these results, it should be pointed out that the statistical significance is mainly affected by the small size of analysis sample, rather than by the size of the model sample. As a consequence, three-member ensembles provide satisfactory estimates of the model climate for the purposes of our study.

Figure 1 shows the global field of 500 mb height t-values for all four model cycles considered in this study. The contours 2.1 and 2.9 correspond to 95% and 99% confidence levels respectively. The sign of the t-value is ignored, because we are primarily interested in the magnitude of the t-statistic. In CY36 (Fig. 1a), the largest t-values are found in the subtropics of both hemispheres and in the southern high-latitudes. The northeastern part of North America is an additional region with prominent t-values, and somewhat weaker values are seen over eastern Asia and around the Bering Strait.

In CY46, t-values in the subtropics are somewhat reduced and in the tropics are dramatically increased (Fig. 1b). In the latest two cycles, CY48 and 12r1, the tropical t-values continue to dominate, and over much of the extratropics t-values are reduced below 95% confidence level. In other words, the emphasis in the model systematic error has shifted from the extratropics in CY36 towards the tropical regions in the later cycles.

Figure 1 indicates that for large parts of the globe there is, in statistical sense, a relatively good agreement between the model climate and verifying analysis. This is true in particular for CY48 and 12r1, whereas the poorest agreement is for CY46.

4 Model errors in upper-air fields

4.1 Wintertime circulation

The model error maps (simulated ensemble mean minus analyzed mean) of 500 mb height for the DJF season in the Northern and Southern Hemisphere are shown in Fig. 2. In the Northern Hemisphere, the error pattern and error amplitude in CY36 and CY46 are very similar (Fig. 2a, b). A strong positive-negative error dipole over the northern Pacific-Alaskan region, which indicates a model tendency to smooth out planetary scale waves, is greatly reduced in CY48 (Fig. 2c) and further reduced in 12r1 (Fig. 2d). This is due to a stronger and more realistic ridging in the 500 mb flow over the Alaskan region in CY48 and 12r1 than in CY36 and CY46 (not shown). Whereas in the two earlier model cycles the Pacific jet extends too far east (thus indicating too strong zonal flow), in CY48 a weaker north-south gradient over the eastern Pacific is associated with an enhanced diffluence and a stronger northerly flow component downstream into the North American mainland. In 12r1, the meridional gradient in the eastern Pacific is weakened even further.

Over the eastern Atlantic-European region, the trough-to-ridge amplitude of the error dipole in Fig. 2 is slightly weaker in CY48 relative to the earlier cycles, and the gradient in the error field between Iceland and the western Mediterranean is weakened as well. This error dipole has been strengthened in 12r1 (Fig. 2d), thus indicating a stronger Atlantic jet than in the analysis. This Atlantic jet intensification is associated with a somewhat deeper low over the Canadian Arctic in 12r1 relative to the earlier cycles.

In the Southern Hemisphere, a different model behaviour is found (Fig. 2e–h). A large reduction in mod-

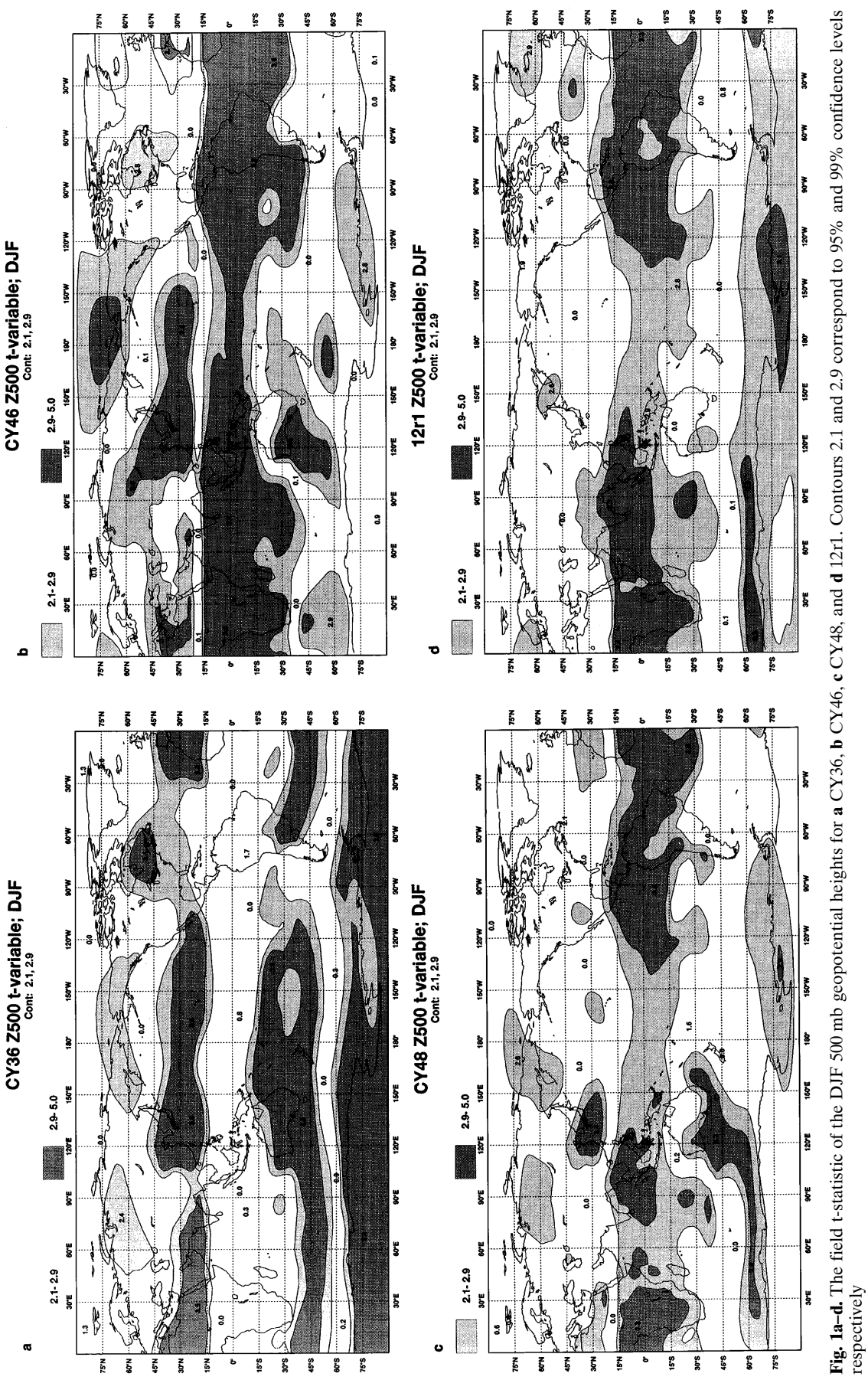

Fig. 1a–d. The field t-statistic of the DJF 500 mb geopotential heights for **a** CY36, **b** CY46, **c** CY48, and **d** 12r1. Contours 2.1 and 2.9 correspond to 95% and 99% confidence levels respectively

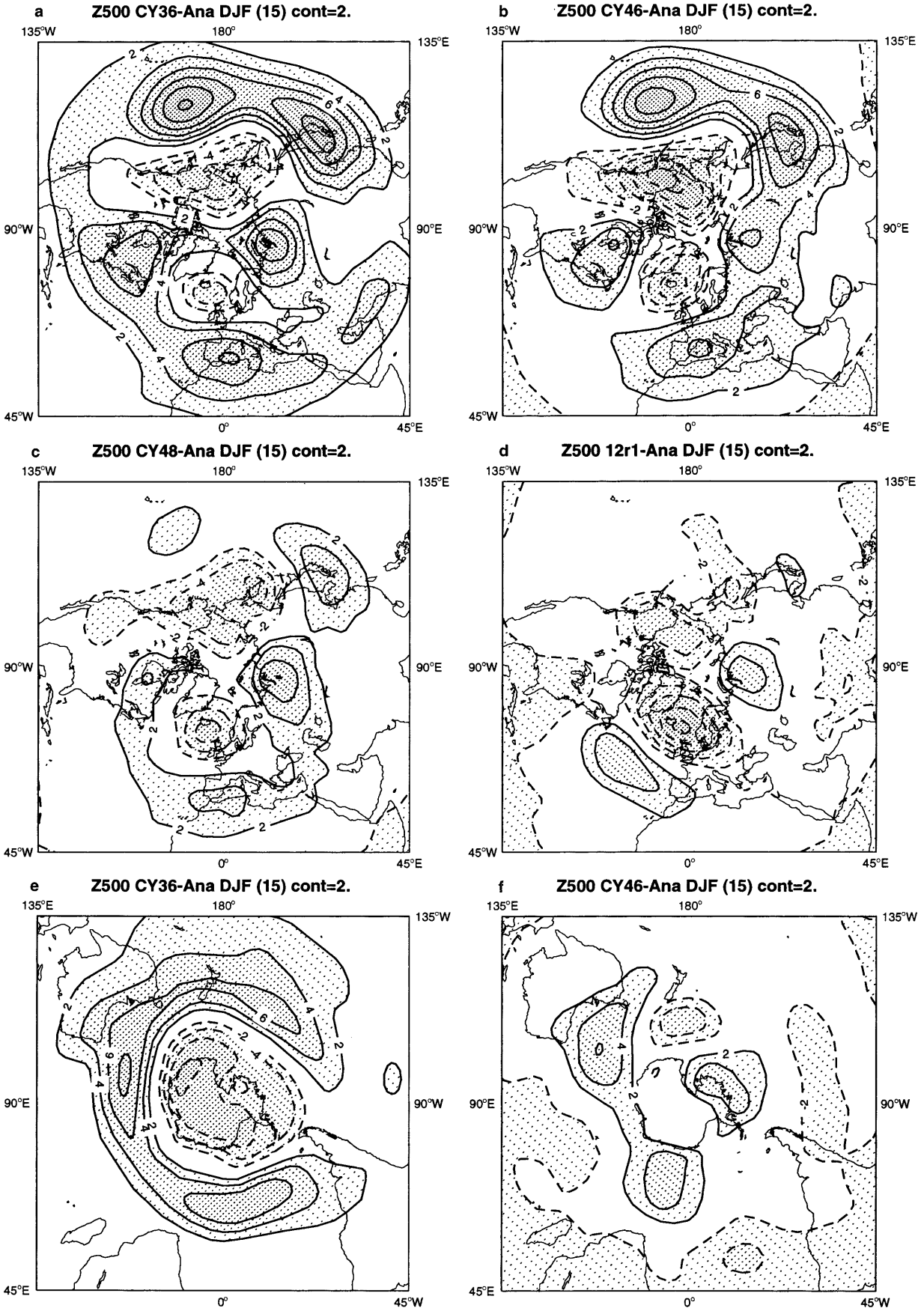

Fig. 2a–h. Northern Hemisphere ensemble mean error fields of DJF 500 mb height for model cycle: **a** CY36, **b** CY46, **c** CY48, **d** 12r1. **e** to **h** as **a** to **d** but for the Southern Hemisphere. *Solid lines* positive errors, *dashed lines* negative errors. Contours every 2 dam

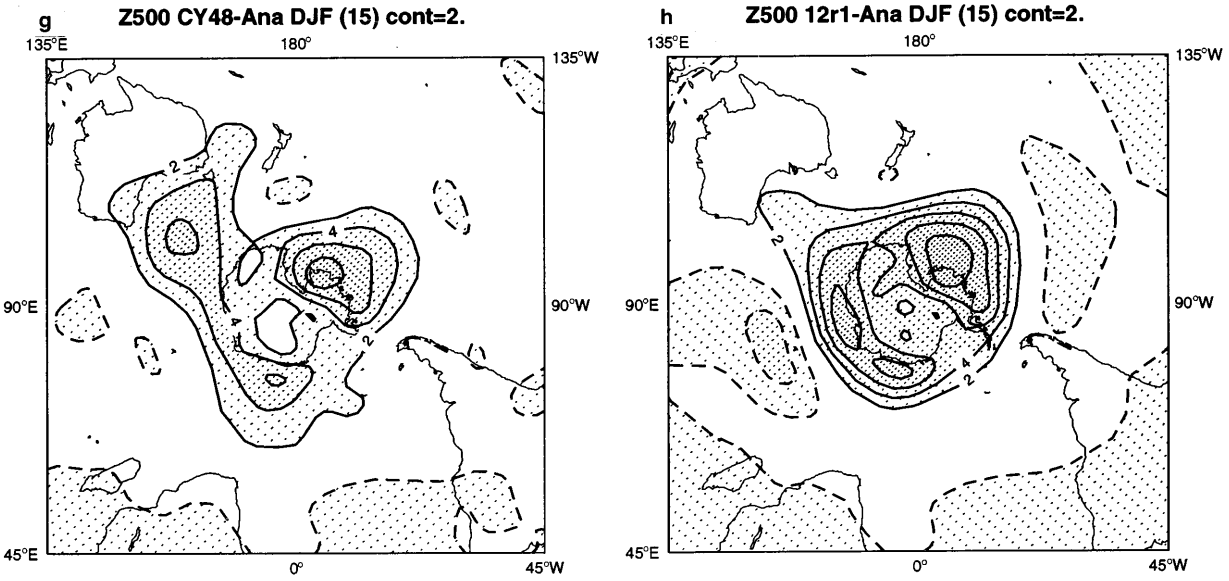

Fig. 2. (Continued)

el error is seen from CY36 to CY46. The error pattern in Fig. 2e indicates that CY36 overestimates the circumpolar vortex (also discussed by Branković and Ferranti 1992). CY46 makes this vortex more realistic, while both CY48 and 12r1 show a tendency to further decelerate the southern circulation so that it is underestimated in these two cycles. In CY46 and CY48 a weak negative geopotential height error dominates in low-latitudes and is slightly more negative in 12r1.

It was noted in Sect. 2.2 that one of the effects of CY46 changes, the reduction in the radiative cooling by high clouds, was especially evident in summer hemispheres. This may explain why CY46 shows an improvement over CY36 in the Southern but not simultaneously in the Northern Hemisphere. The impact of the revised cloud shortwave optical properties introduced with CY46 is strongly seasonally dependent, i.e. their beneficial impact is primarily seen in the summer hemisphere over the high-latitude region with semipermanent daylight when the absorption of solar radiation by the high-level clouds is strongest. However, other changes introduced between CY36 and CY46 may have contributed to such an improvement as well.

Hemispheric differences in the error pattern at 1000 mb (not shown) are similar to those at 500 mb. In the Northern Hemisphere, the main improvement in CY48 comes from a better representation of the subtropical high between the Hawaiian Islands and the western coast of North America. In CY36 and CY46 this high was overestimated, displacing the Aleutian low too far north and causing strong surface westerlies over the northeastern Pacific. Despite the fact that the Atlantic subtropical high is better simulated in 12r1 than in the other cycles, the north Atlantic/European surface westerlies are found to be overestimated. This is mainly due to a somewhat too deep Icelandic low in 12r1. (Additional discussion on model mean height errors with respect to interannual variation is given in Sect. 7.2.)

The error structure in zonally averaged zonal wind (Fig. 3) is consistent with the height error pattern discussed already. In the Northern Hemisphere in all cycles, a positive u-wind error north of 30°N, and a negative error in the subtropics and tropics, are mainly a consequence of poleward displacement of the wind maximum relative to the analysis. Although a northward shift is seen in all model cycles, it is smallest in 12r1. In both CY48 and 12r1 the Northern Hemisphere westerly error is confined to the upper troposphere and lower stratosphere. However, in cycle 12r1, the polar night jet near the top of the model is too strong and consequently the westerly error is larger than in the other cycles. A relatively large negative error in the tropics at the tropopause level in CY46 (Fig. 3c) accounts, in addition to the jet poleward shift, for too strong tropical easterlies (seen to a much lesser degree in the other three model cycles).

In the Southern Hemisphere, a large westerly error in CY36 is, similar to the Northern Hemisphere, a consequence of both strengthening of zonal wind and its poleward displacement. In all later model cycles this error is greatly reduced and reflects the progressive deceleration of the circumpolar vortex with each cycle (see also Fig. 2e–h).

The error in the model eddy kinetic energy is gradually reduced with each cycle, especially in the tropical upper troposphere and lower stratosphere (not shown). A large positive error in eddy kinetic energy in the Southern Hemisphere midlatitudes in CY36 is very likely associated with large error in zonally averaged circulation (Fig. 3b).

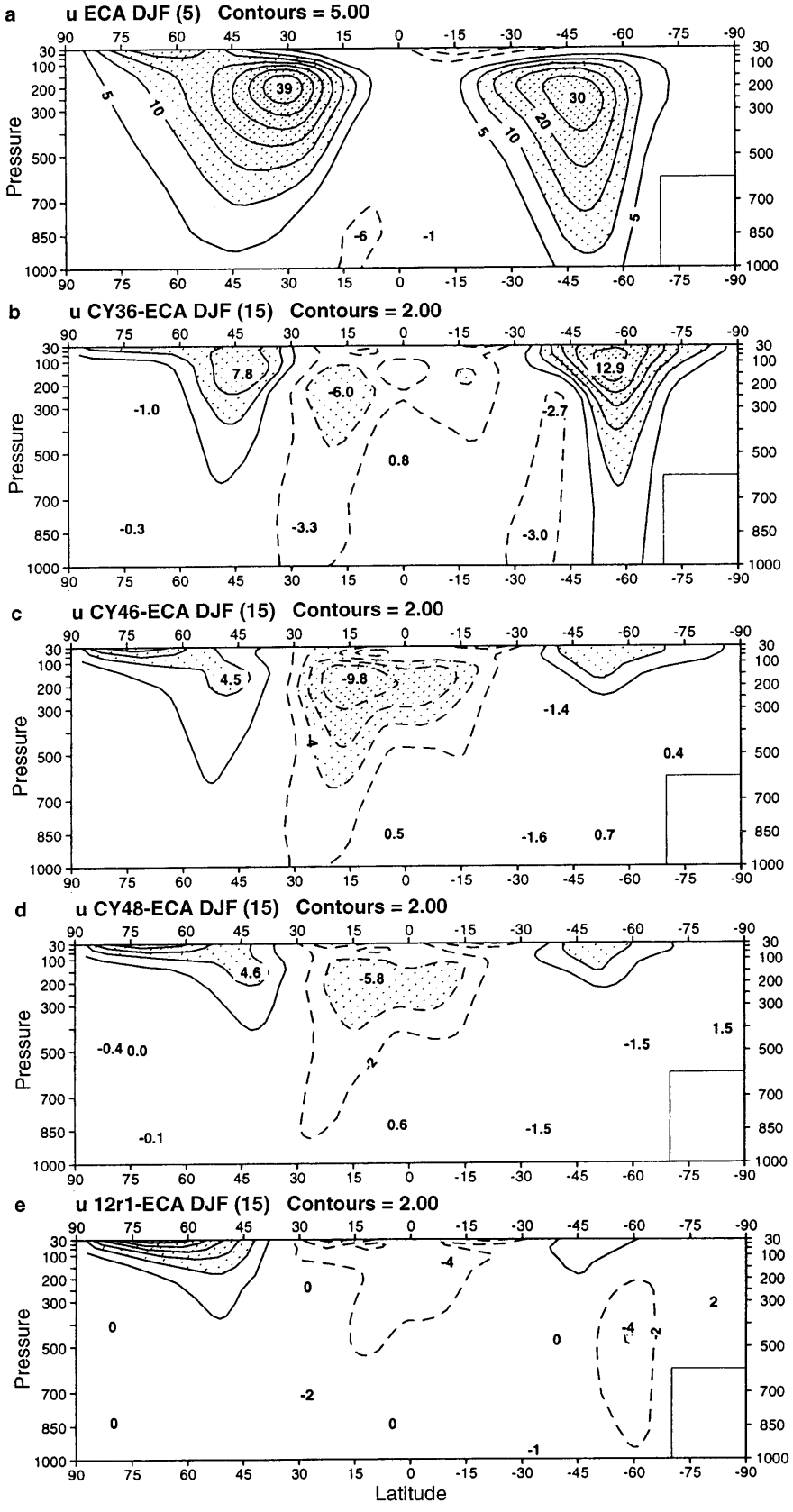

Fig. 3a–e. Zonally averaged cross sections of ensemble mean DJF zonal wind for: **a** ECMWF analysis 5-year mean. Errors for model cycle: **b** CY36, **c** CY46, **d** CY48 and **e** 12r1. *Solid lines* westerlies and positive errors, *dashed lines* easterlies and negative errors. Contours every 5 ms^{-1} in **a** and every 2 ms^{-1} in **b–e**

4.2 Temperature errors

The error pattern in zonally averaged temperature has been substantially changed from one model cycle to the other (Fig. 4). In the model tropical upper atmosphere, a very small error in CY36 (Fig. 4a), is modified to relatively large errors in CY46, alternating in sign with height (Fig. 4b). Such an error pattern, but with somewhat reduced amplitude is also found in CY48 (Fig. 4c), while in 12r1 (Fig. 4d) the warming of the model tropical upper atmosphere reaches as much as 5 K. It seems plausible to ascribe some of these errors, in particular warming above 150 mb, to the changes in radiation and cloud parametrization introduced with CY46, as discussed in Sect. 2.2. Indeed, a similar error pattern in the tropical stratosphere as in Figs. 4b–d is seen at mean forecast day 10 (D10) for March 1993 ECMWF operational forecasts (not shown). In January 1993, i.e. prior the introduction of the CY46 changes, D10 upper atmosphere temperature error pattern was different from that in Fig. 4b with a weak cooling throughout the tropical upper troposphere and lower stratosphere.

In Fig. 4 in the polar stratosphere of both hemispheres, a large negative temperature error is seen, the error being larger in the summer hemisphere. While the erroneous cooling in the Northern Hemisphere is almost unchanged in various model cycles, in the

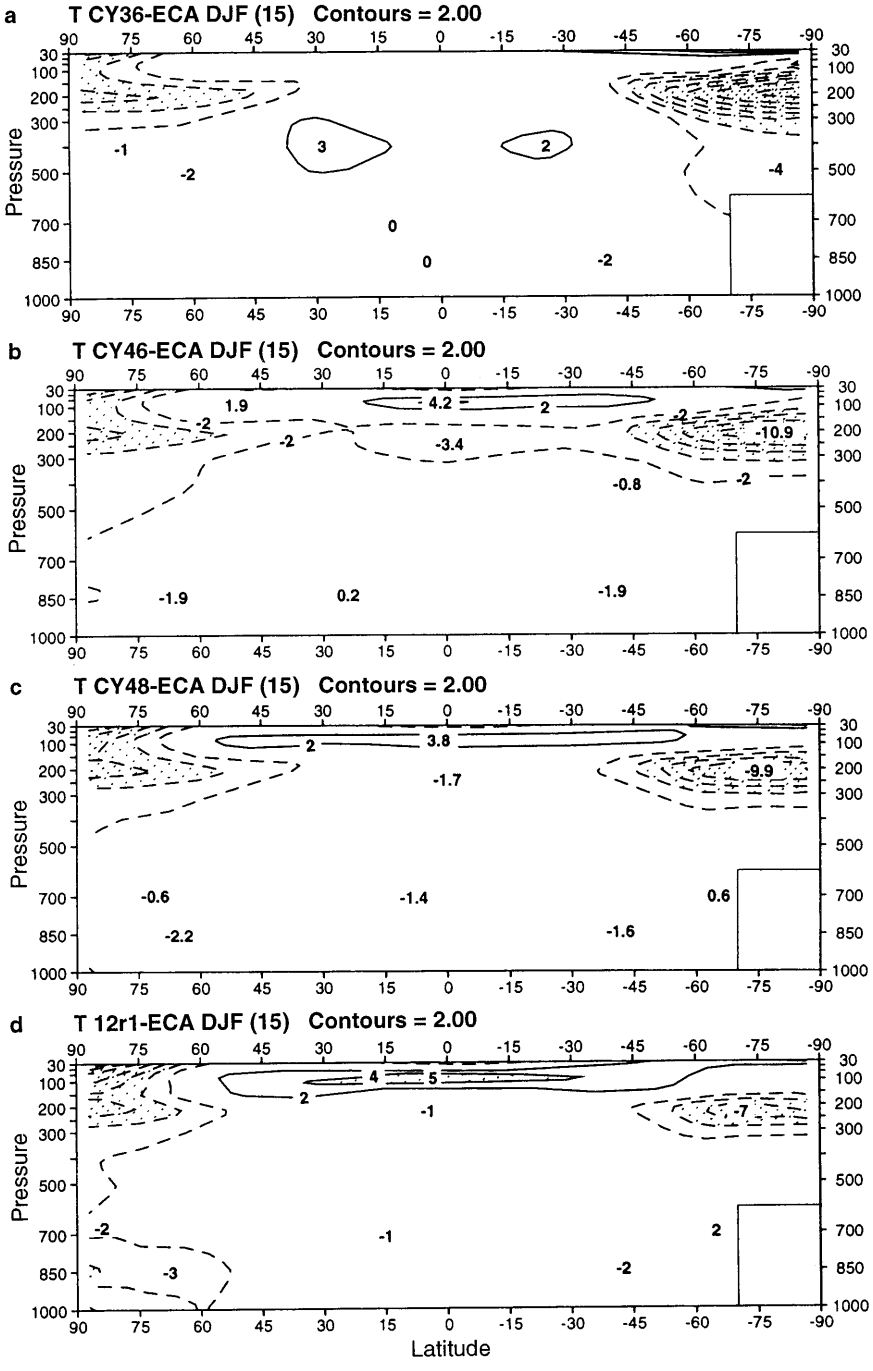

Fig. 4a–d. Zonally averaged cross sections of ensemble mean DJF temperature error for model cycle: **a** CY36, **b** CY46, **c** CY48 and **d** 12r1. *Solid lines* positive errors, *dashed lines* negative errors. Contours every 2 K

Southern Hemisphere it has been reduced by about 7 K (or nearly 50%) from CY36 to 12r1. This polar stratospheric cooling is a common feature of many GCMs and its origin is not well understood (Boer et al. 1991). Lary and Balluch (1993) suggested that taking into account the effects of spherical geometry in the parametrization of radiation processes (rather than the plane parallel approximation used by almost all GCMs) would significantly reduce the underestimation of the solar heating rate, especially in polar regions. However, in the case of the ECMWF model, the changes to the formulation of physical parametrization are partly responsible for the reduction of this error from CY46 to 12r1. Some of the beneficial impact seen in the cycle 12r1 polar stratospheric temperature error may have come from the improved vertical resolution in this model cycle. This is suggested by comparing zonally averaged temperature errors in the medium-range for the 19-level T63 control (unperturbed) forecasts from the ECMWF ensemble prediction system against 31-level operational T213 forecasts. The 19-level model has a stronger cooling in the DJF southern polar stratosphere than 31-level model.

4.3 Mean meridional circulation

For reasons of space, mean meridional circulation comprising zonally averaged vertical and meridional velocities will be discussed without displaying figures.

In successive model cycles, the intensity of the DJF lower tropospheric large scale ascent (centred in the analysis at about 5°N and mainly associated with the Pacific intertropical convergence zone, ITCZ), is progressively increased and its positioning is shifted slightly northwards. This increase varies between about 15% relative to analysis in CY46 to over than 70% in 12r1. (Note, however, that the operational analysis itself may be deficient in this respect, since it was performed using much earlier cycles of the forecast model.) At the same time, the intensity of the upper tropospheric ascent at about 10°S, that can be associated with the south Pacific convergence zone (SPCZ), and the intensity of the descending branch of the Hadley cell between 15 and 20°N do not change significantly in the model (apart from CY46 where the upper air ascent is much weaker than in the other models and analysis). Thus the strengthening of the vertical circulation in the Hadley cell, seen especially in CY48 and 12r1, is primarily due to the enhancement of rainfall within the Pacific ITCZ (see Sect. 6).

The outflow branch of the zonally averaged meridional wind is weakest in CY46, but is steadily increasing in the later cycles thus indicating an overall strengthening of the Hadley circulation. It is interesting to note that, when compared with the analysis, all model cycles show a strengthening of the thermally indirect Ferrel cell, the strongest being in CY36. This is associated with an increased eddy momentum flux convergence in the model, which in turn is associated with an overall enhancement in eddy momentum flux (not shown). Such an increase is most pronounced in CY36, where the eddy momentum flux error in the Southern Hemisphere middle latitudes amounts to about 50% of the analysis maximum.

4.4 High-frequency variability

Figure 5 shows standard deviation of DJF 500 mb heights for the high frequency range (HF) with a period shorter than 10 days. Essentially, it represents locations of jet streams and major storm tracks.

The Northern Atlantic maximum is well represented in the model, and 12r1 (Fig. 5e) has the amplitude closest to the analysis (Fig. 5a). Over northern Europe and northern Asia the HF variability is underestimated by the model, possibly indicating insufficient penetration of northern Atlantic storms into the Eurasian continent. Although a secondary maximum at 60°E, 55°N is seen in each model cycle, its amplitude is reduced relative to the analysis.

In the northern Pacific, the analyzed HF has its maximum close to the date line. In this region variability is generally underestimated by all model cycles. In the earlier two cycles, an overestimation of HF in the eastern Pacific region points to a too strong jet extending from the central into the eastern north Pacific and North America. Whilst a relative minimum over North America, between the two storm-track regions, is represented reasonably well in the model, the Arctic minimum is overestimated.

4.5 The largest differences between successive cycles

In this section we focus on some of the DJF ensemble mean difference fields between CY48 and CY46, because they were found to be the largest differences between successive cycles. As indicated in Sect. 2 and Table 1, CY46 changes were related to cloud and radiation parametrization, whereas CY48 changes were mainly in the parametrization of soil processes and PBL.

Figure 6 indicates a relative change from CY46 to CY48 for 500 mb height, 850 mb temperature and 850 mb relative humidity. The enhanced ridging over the Alaskan region in CY48 is seen as a positive difference in Fig. 6a. This positive difference extends throughout northern polar latitudes, thus implying an overall increase of geopotential height in CY48. Over the Canadian Arctic, this increase results in a more realistic semi-permanent low, which was too deep in CY46. However, over northwestern Siberia, this positive difference implies a weaker trough, which in turn contributes to a weakening of the wave number 3 pattern in high-latitudes.

Negative differences over the Northern Pacific are indicative of a more realistic trough-ridge system over the eastern Pacific/Alaskan region in CY48. However, the extension of these negative differences into eastern Asia indicates a deepening of the trough over the

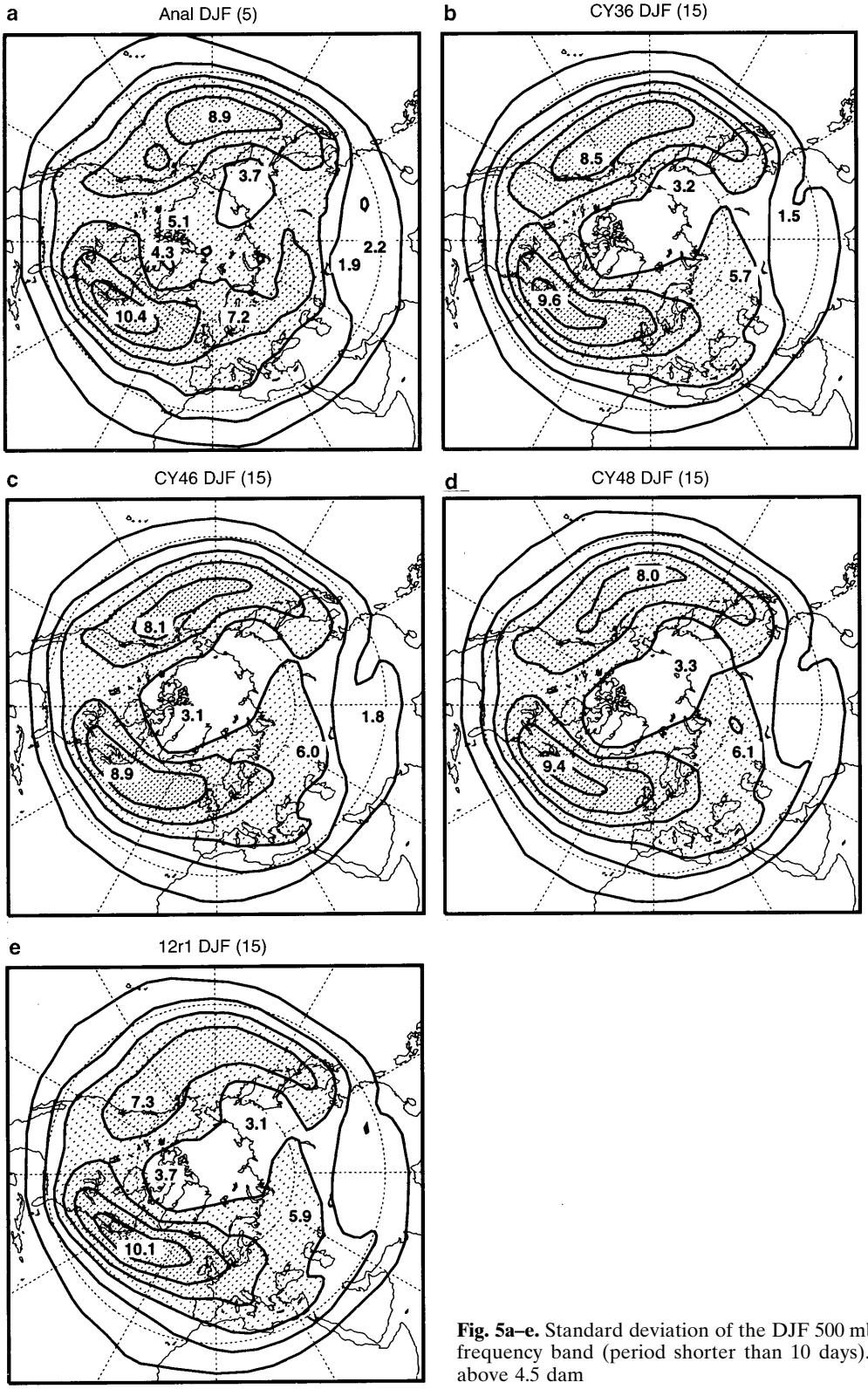

Fig. 5a–e. Standard deviation of the DJF 500 mb geopotential heights for the high-frequency band (period shorter than 10 days). Contours every 1.5 dam, *shading* above 4.5 dam

Kamchatka peninsula and strengthening of the jet off the coast of Japan. Negative differences over much of North America indicate a more realistic simulation of the trough over the eastern USA with CY48.

For 850 mb temperature (Fig. 6b), the difference pattern between CY48 and CY46 over the north Pacific/Alaskan region is consistent with the height differences in Fig. 6a. The cooling over the north Pacific is not necessarily a deficiency of CY48. According to the ECMWF re-analysis project experimentation, the analysis based on model cycle 48 (which fits observations better), would be cooler over the north Pacific in com-

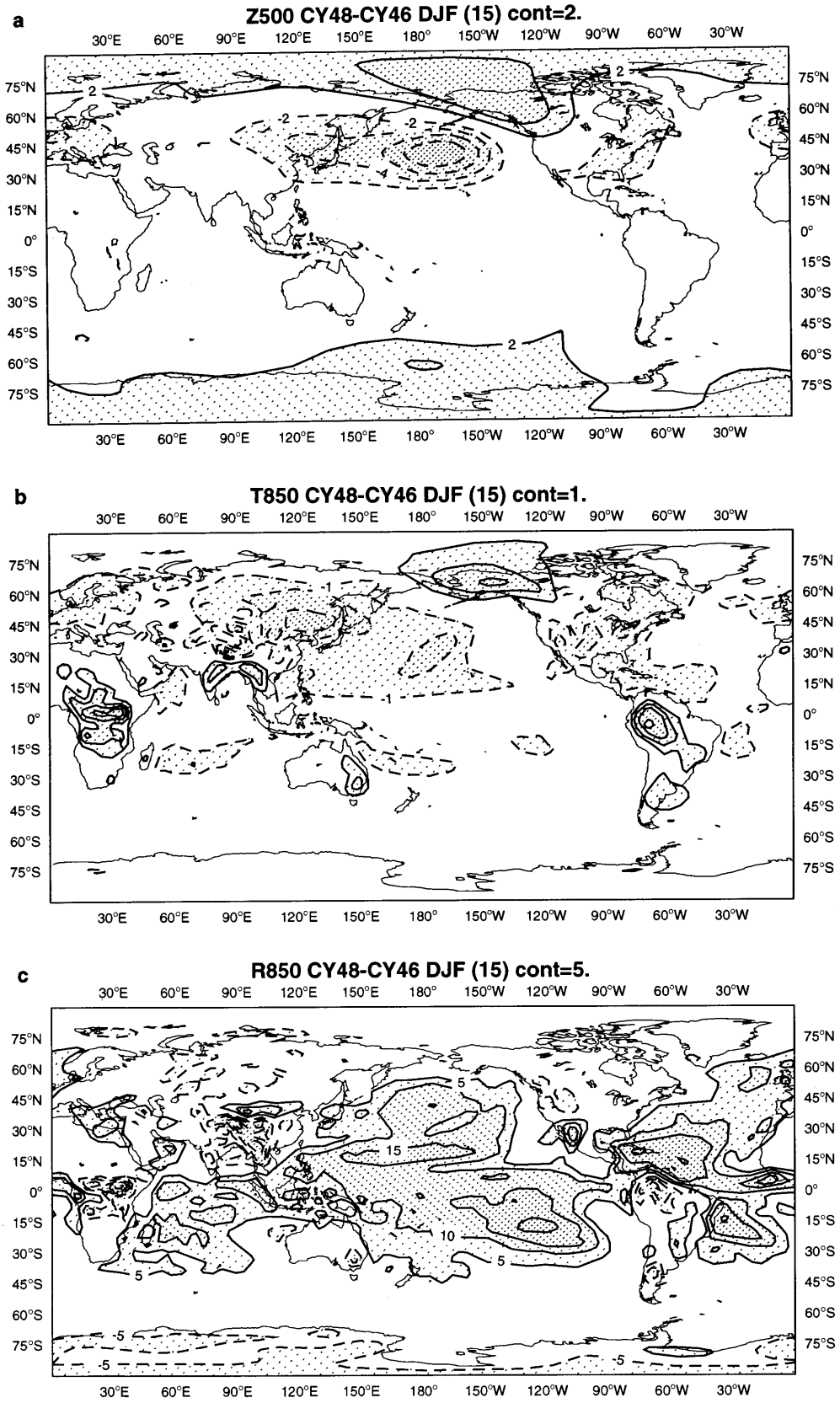

Fig. 6a–c. Ensemble mean DJF difference fields for CY48 minus CY46: **a** 500 mb height, **b** 850 mb temperature and **c** 850 mb relative humidity. *Solid lines* positive differences, *dashed lines* negative differences. Contours every 2 dam in **a**, 1 K in **b** and 5% in **c**

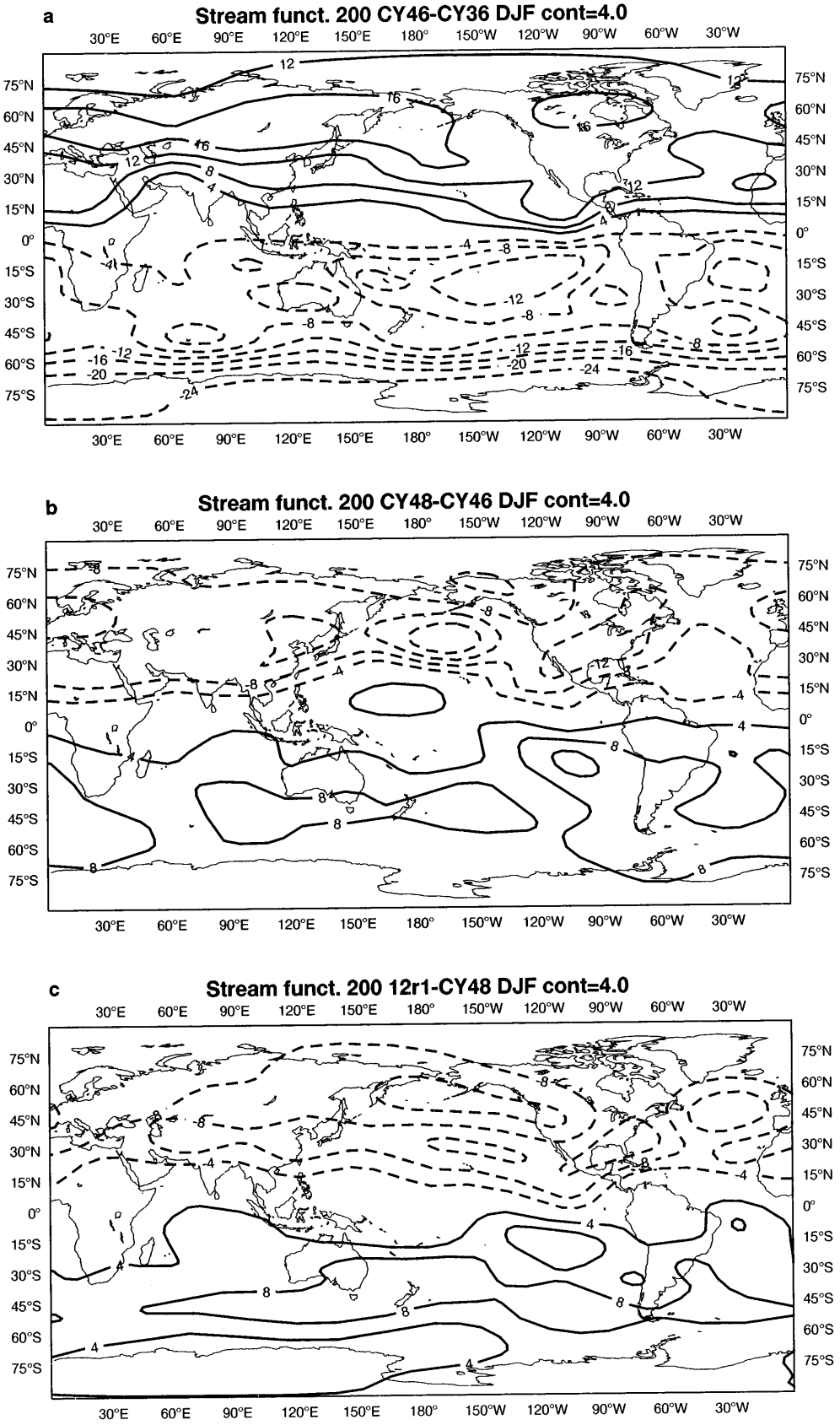

Fig. 7a–c. Ensemble mean DJF 200 mb stream function difference fields for **a** CY46 minus CY36, **b** CY48 minus CY46 and **c** 12r1 minus CY48. *Solid lines* positive differences, *dashed lines* negative differences. Contours every 4×10^6 $m^2 s^{-1}$

parison with analysis based on model cycle 46 (Per Kållberg, ECMWF re-analysis project, personal communication). Thus, negative temperature differences seen over much of the north Pacific would imply reduced errors in CY48 with respect to an improved analysis.

A striking feature in Fig. 6b is a warming of tropical and subtropical continents in CY48, with maxima in tropical South America and Africa exceeding 4 K. Closely related to such a difference pattern is drying over the same regions (Fig. 6c). Because of its confinement to the land points, it seems likely that the cause for such a difference pattern is the new scheme for soil processes rather than the other changes introduced with CY48.

A large change in relative humidity at 850 mb over the oceans in Fig. 6c can be, on the other hand, attributed to a small but significant increase in the height of PBL. The entrainment at the top of PBL, introduced with CY48, makes (on average) the model PBL deeper relative to the depth of PBL in the previous cycles. The pressure level of 850 mb is (because of its proximity to the top of PBL) on average more frequently below the inversion level rather than in the drier air above.

The tropical upper troposphere geopotential height significantly decreased from CY36 to CY46 (not shown). This remarkable decrease on the tropical planetary scale is associated with a cooler tropical upper troposphere in CY46 relative to CY36 (see Fig. 4b and 4a). In terms of stream function differences, the 200 mb equatorial easterlies in CY46 have increased and weak westerlies have decreased relative to CY36 (Fig. 7a; see also Fig. 3b, c). With the introduction of CY48 the tropical heights recover, with the tendency to further increase in 12r1, which is consistent with a relative warming around the tropopause in the latter two cycles. The stream function differences in Fig. 7b, c exhibit reversed signs when compared to Fig. 7a. The 12r1 westerlies in the eastern tropical Pacific are comparable with the analysis wind field.

5 Circulation regime statistics

5.1 Frequency of blocking

Atmospheric blocking is a phenomenon that has been continuously scrutinised at ECMWF in the context of operational analyses and forecasts. The assessment of frequency of blocking, both analyzed and modelled, is important in the diagnosis of atmospheric low-frequency variability and model performance. Our statistic of blocking frequency is based on the computation of blocking index described by Tibaldi and Molteni

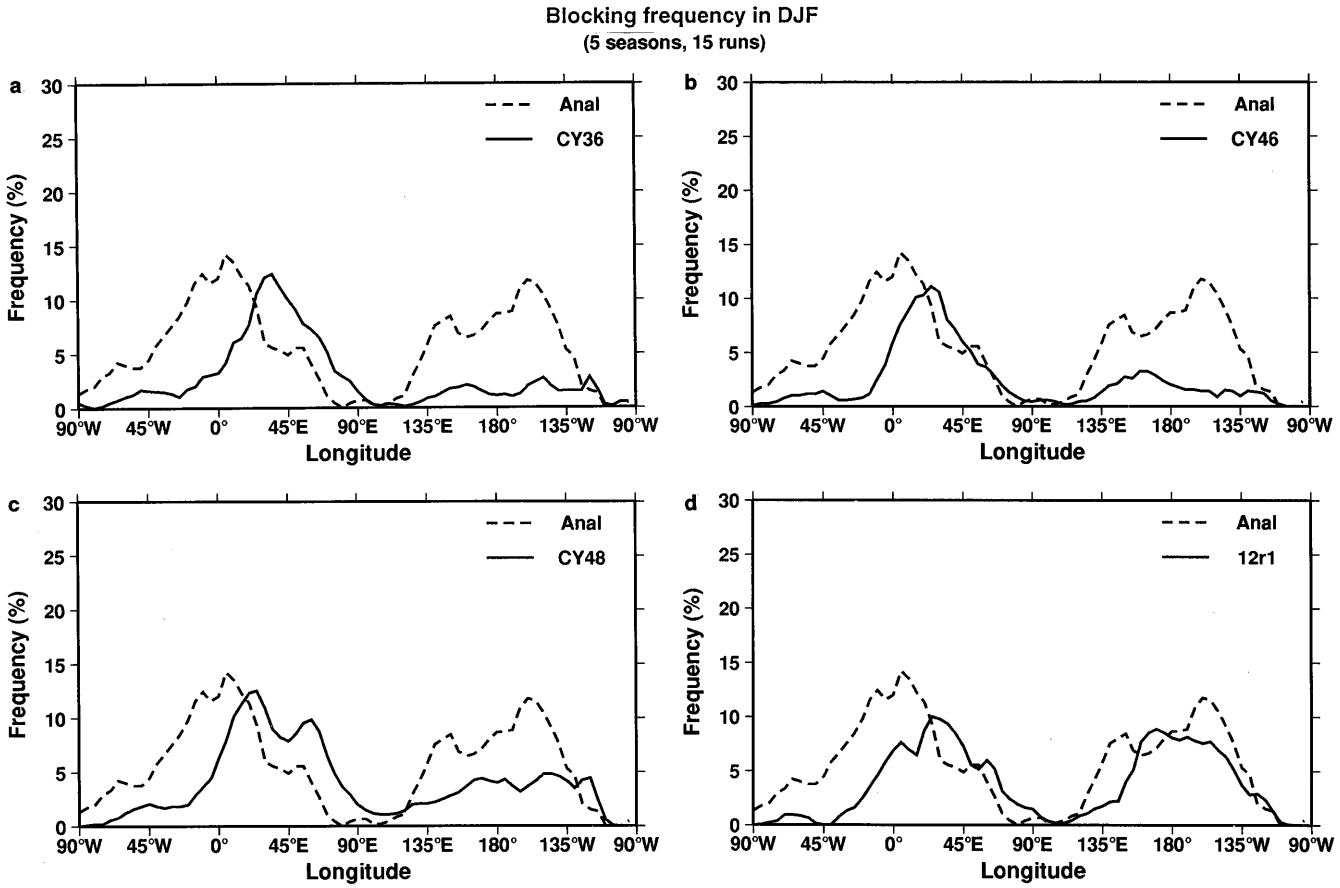

Fig. 8a–d. Frequency (in %) of occurrence of blocking as defined by Tibaldi and Molteni (1990) for DJF ensembles of model cycle: **a** CY36, **b** CY46, **c** CY48 and **d** 12r1. *Dashed lines* 5-year analysis mean

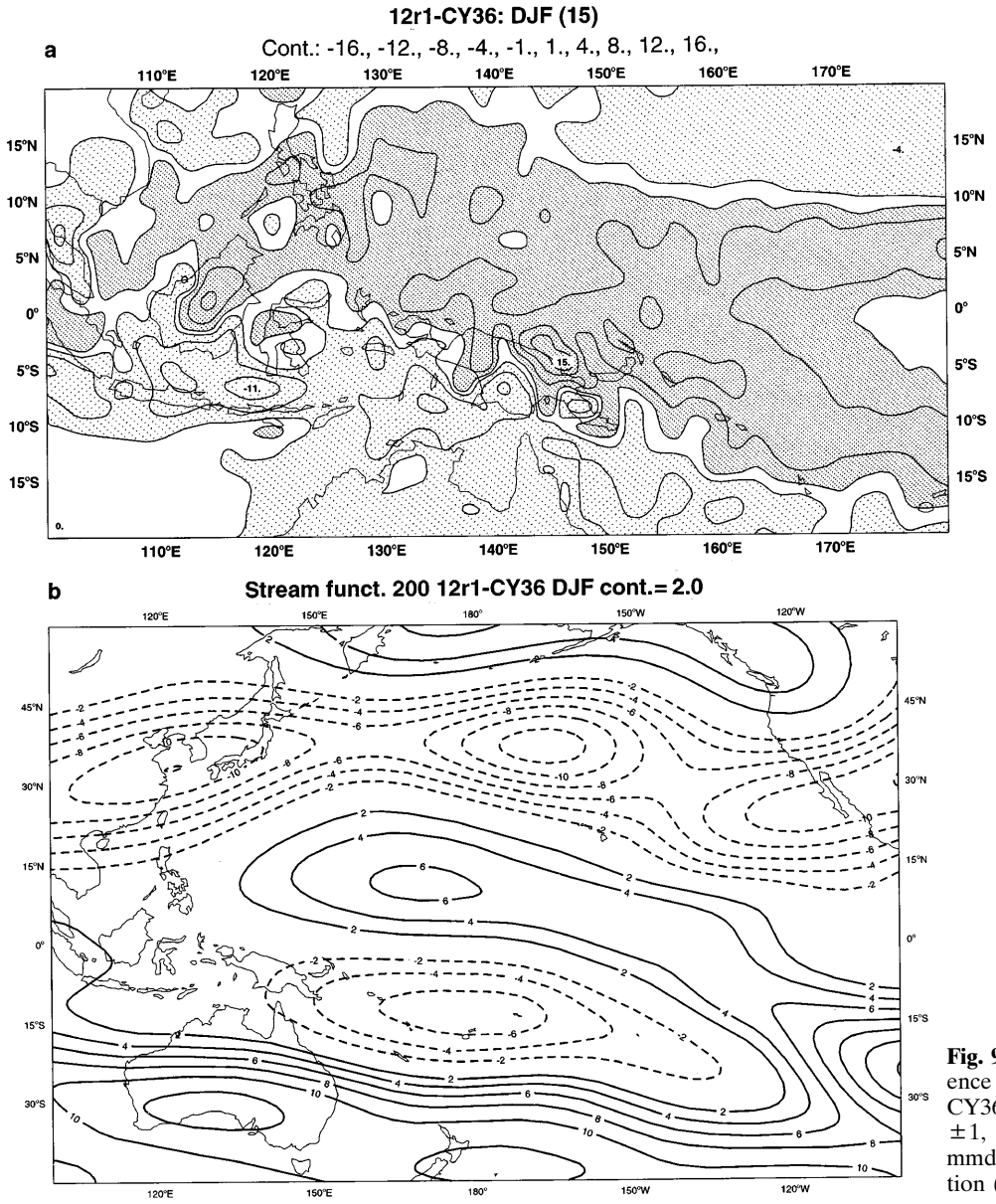

Fig. 9a, b. Ensemble mean DJF difference fields between cycle 12r1 and CY36 for **a** precipitation, (contours ± 1, ± 4, ± 8, ± 12 and ± 16 mmday^{-1}), and **b** 200 mb stream function (contours every 2×10^6 m^{2}s^{-1})

(1990). The method essentially utilizes gradients in the 500 mb heights defined for the "northern" and the "southern" parts of a predefined latitude band. The flow at a given point is defined as "blocked" if the southern height gradient is positive, or/and the northern height gradient is weaker than -10 m/deg lat. The choice of the latitude belt, for which the computation of blocking index is performed, is somewhat arbitrary, so the method may not be considered as fully objective.

Figure 8 shows frequency of blocking occurrence, as defined by Tibaldi and Molteni (1990), averaged over the five winters of experimentation. The analyzed frequency (dashed line) has two main maxima, one over the Atlantic/European region and another over the eastern Pacific. In all four model cycles, the amplitude of the Atlantic maximum is relatively close to the analysis value, but its position is displaced eastward. This eastward model bias suggests that the mean flow pattern over the central and eastern Atlantic has changed very little from one model cycle to the next; the Atlantic jet is still overestimated in the model and penetrates too far east, thus shifting the region of upper-air diffluence into the European continent. A relative improvement in CY48 and 12r1 is seen further east where the location of the secondary maximum at 60°E (the Ural mountains) is reasonably well captured in 12r1, but has a much overestimated amplitude in CY48. In 12r1, in addition to the eastward shift, the Atlantic maximum has been weakened relative to the analysis and to the other cycles. This deterioration in the representation of blocking frequency can be associated with the strengthening of the Atlantic jet as discussed in Sect. 4.1. This is consistent with the results of Kaas and Branstator (1993), who found that the diffluence over the Atlantic (and consequently the percentage of blocks) in the NCAR CCM simulations is greatly reduced when the model was forced toward the zonal

mean state that corresponds to anomalously zonal flow.

Over the Pacific region CY36 and CY46 substantially underestimate the frequency of blocking occurrence. This deficiency is somewhat alleviated with CY48. In view of the discussion in Sect. 4.1, this improvement should be associated with a better representation of the 500 mb ridge in the northern Pacific/Alaskan region and the reduction of the model errors in CY48. We note that in their famous study of the 1977 winter, Miyakoda et al. (1983) showed that sensitivity of their model to the treatment of PBL was critical for a successful simulation of the Pacific blocking event. Further reduction of the model mean error over the north Pacific seen in Fig. 2d, together with a realistic low-frequency variability (not shown) reflect as a substantial improvement in the representation of blocking in 12r1 (Fig. 8d).

An argument based on a study by Ferranti et al. (1994b) may explain why 12r1 shows a strong improvement in frequency of blocking over the North Pacific. Based on experimental evidence, they found that the strongest impact on the modelled blocking activity in both Pacific and Atlantic/European regions was due to an increase of quasi-stationary diabatic heating over the western tropical Pacific. Such an increase in diabatic heating was introduced into their experiments via an idealized strong positive SST anomaly defined in the Indonesian region, which caused an increase in rainfall over the western tropical Pacific.

Mullen (1989) has found that the *combination* of Pacific SST anomalies, a warm anomaly in the tropical Pacific and a cool anomaly in the extratropical Pacific, was more effective in modifying blocking activity over the midlatitude northern Pacific than either anomaly acting alone. However, in contrast to Ferranti et al. (1994b) his warm SST anomaly was positioned further to the east, over the central and eastern equatorial Pacific.

The difference in the rainfall between 12r1 and CY36 in the western Pacific is shown in Fig. 9a. A relatively large area of positive differences exceeding 4 mm/day (dense stippling) is found over much of the western tropical Pacific (including Borneo, the Philippines and parts of Papua/New Guinea). This increase in the 12r1 rainfall amount may be viewed as an equivalent to the increase in diabatic heating in the Ferranti et al. (1994b) study. However, unlike their experiments, this increase cannot be linked to changes in the local SST forcing, since the SST fields in CY36 and 12r1 were essentially identical. Therefore, an increase in 12r1 rainfall over Indonesia must be attributed to an improved model efficiency in exploiting existing SST forcing.

This is demonstrated in Fig. 9b, where the corresponding difference for the 200 mb stream function between 12r1 and CY36 is shown. In the tropical Pacific, the upper-air difference flow pattern is typical of Gill's (1980) linear model forced steady solution. The positioning of a pair of anticyclones, straddling the equator, corresponds to the region of maximum precipitation difference in Fig. 8a (east of Papua/New Guinea and close to the equator). This flow pattern can be interpreted as the model tropical response to a steady low-level diabatic heating on the equator.

In the northern central Pacific, the difference in the stream function indicates the strengthening of the jet in 12r1 relative to CY36 between 20° and 30°N and its weakening along 50°N. The deceleration of the Pacific jet in mid-latitudes is consistent with the increase in the frequency of blocking over the Pacific region (Fig. 8d). Miyakoda and Sirutis (1990) also found that a more sophisticated version of the GFDL model, which included relatively complex physical parametrizations, improved the representation of blocking activity when compared with a model version with a simpler physics. They suggested that a successful simulation of blocking was associated with a displacement of the upstream westerlies towards lower latitudes.

Finally, it should be remembered that the result in Fig. 9 shows a cumulative effect of the modifications introduced between CY36 and 12r1, and the rainfall increase in Fig. 9a should not be ascribed to the 12r1 changes alone.

5.2 Planetary-wave regimes

The ability of the different model cycles to reproduce low-frequency variability in the planetary scale flow is tested by evaluating the frequency of occurrence of the five main regimes of 500 mb planetary waves defined by Molteni et al. (1990) from a 32-winter record of 500 mb height analyses. The regimes were defined as clusters associated with local maxima in the probability distribution of the projections of eddy fields onto three rotated empirical orthogonal functions (REOFs). Following Ferranti et al. (1994a), the projections onto these three REOFs have been computed using running 5-day mean anomalies from the 15 model integrations, and each field has been classified in one particular cluster according to the distance between its position in the 3-dimensional REOF space and the position of the centroids of the clusters (the closest centroid has been selected).

A similar classification has been performed on ECMWF analyses from winter 1979/80 to 1990/91; the model frequency will be compared with the analysis frequencies in either this 12-winter sample or in a shorter sample including only the five winters, i.e. those corresponding to the initial dates of the experiments. To test the significance of the comparison with the latter sample, model frequencies in the three separate 5-run sub-samples have also been computed (they included experiments initiated on the same calendar day, i.e. on 1, 2, and 3 November respectively in each year). Given the simpler classification method used here, a comparison with the long-term climatological frequencies from Molteni et al. (1990) is not appropriate. In evaluating these results, we remind the reader that clusters 1 and 2 correspond to anomalies with positive Pacific/North American (PNA) index, clusters 3 and 5 to anomalies with negative PNA index. Clus-

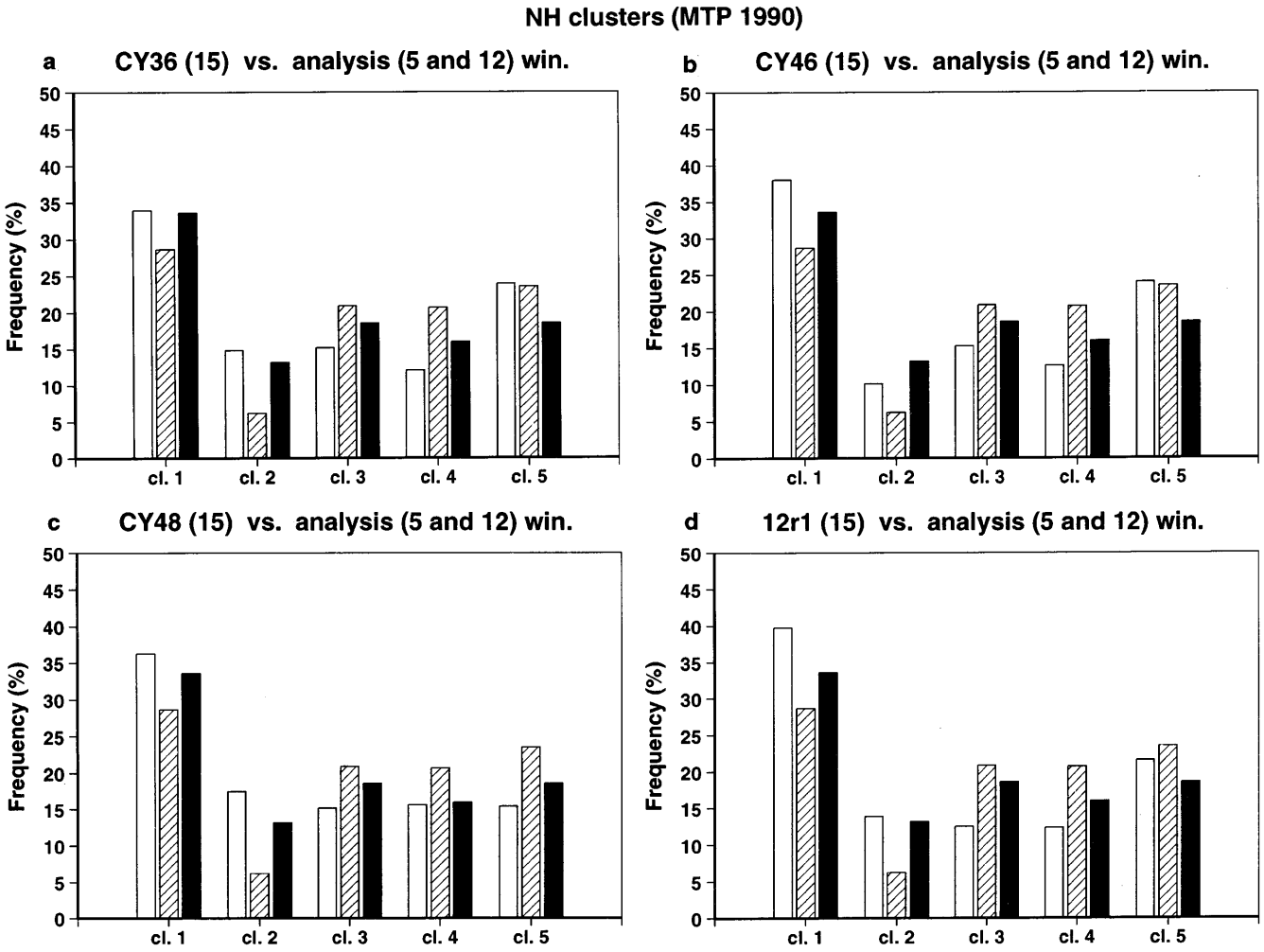

Fig. 10a–d. Frequency (in %) of planetary clusters as defined by Molteni et al. (1990) for DJF ensembles of model cycle (*left-hand, open bars*): **a** CY36, **b** CY46, **c** CY48 and **d** 12r1. *Centre bars* (*hatched*) analysis from 5-year average, *right-hand* (*solid*) bars analysis from 12-year average

ters 2, 4 and 5 represent flows with larger-than-average planetary wave amplitude, while cluster 1 (the most populated) includes fields which are fairly close to the climatological mean state.

The comparison between the modelled frequencies and the analysis frequencies is shown in Fig. 10. For each cluster, the modelled frequencies are shown as the left-hand bars, the 5-year analysis frequencies as the centre bars and the 12-year analysis frequencies as the right-hand bars in Fig. 10.

When compared with the 5-year frequencies in all four model cycles, the frequencies of positive-PNA clusters (1 and 2) are overestimated, while those of clusters 3 and 4 are underestimated. The large frequency of cluster 2 in CY48 is consistent with the strengthening of the ridge over the Rockies documented earlier. The significance of these differences is confirmed by the analysis of model frequencies in the three 5-run sub-samples (not shown), which consistently reproduce the behaviour of the 15-run averages. On the other hand, both CY48 and 12r1 underestimate (the latter only slightly, Fig. 10d) the frequency of cluster 5 with respect to the 5-year analysis, which the previous cycles did not. However, such underestimation is not consistently confirmed by the 5-run sub-samples: very large differences between sub-samples are found for cluster 5 in these two model versions.

If the 12-winter analysis sample is used as a comparison (the right-hand bars in Fig. 10), a better agreement is noticed between analyzed and modelled frequencies for all cycles, and CY48 turns out to give the best results, followed closely by CY36 and 12r1. It can be argued that, since cluster frequencies are subject to considerable sampling errors, the 12-winter sample gives a sounder basis of comparison that the 5-winter one. On the other hand, the 12-winter sample includes the very strong El Niño event of 1982/83, while no cold event of comparable intensity to the 1988/89 La Niña is present. Consequently, the 12-winter sample is more "biased" towards positive PNA anomalies, and this may compensate for model systematic errors. Insofar as the differences between the 12-winter and the 5-winter samples are a real reflection of differences in the boundary forcing, it a cannot be concluded that

CY48 or 12r1 represent an improvement with respect to CY36 in the simulation of planetary wave regimes.

6 Precipitation

The zonally averaged total rainfall amounts for the four model cycles and for the DJF climate (Legates and Willmott 1990) are shown in Fig. 11a. Over much of the globe there is a broad agreement between the cycles studied here. The main difference is the larger tropical precipitation in CY48 and 12r1 than in the two earlier cycles, particularly at 10°N and 10°S which corresponds to the ITCZ and the SPCZ respectively. The largest contribution to such an increase comes from convective precipitation over the oceans (Fig. 11b), which may be attributed to the modification in the parametrization of shallow convection (see Sect. 2 and Table 1). All models show a northward displacement of the ITCZ rainfall relative to the DJF climate. Despite the shift, the later two model cycles undoubtedly represent an improvement over the former two cycles. However, the minimum at the equator is too deep in the model.

In the extratropics, CY36 is the wettest of the four. The largest difference is again due primarily to convective precipitation over the oceans, since the contribution from the large-scale precipitation to total amounts

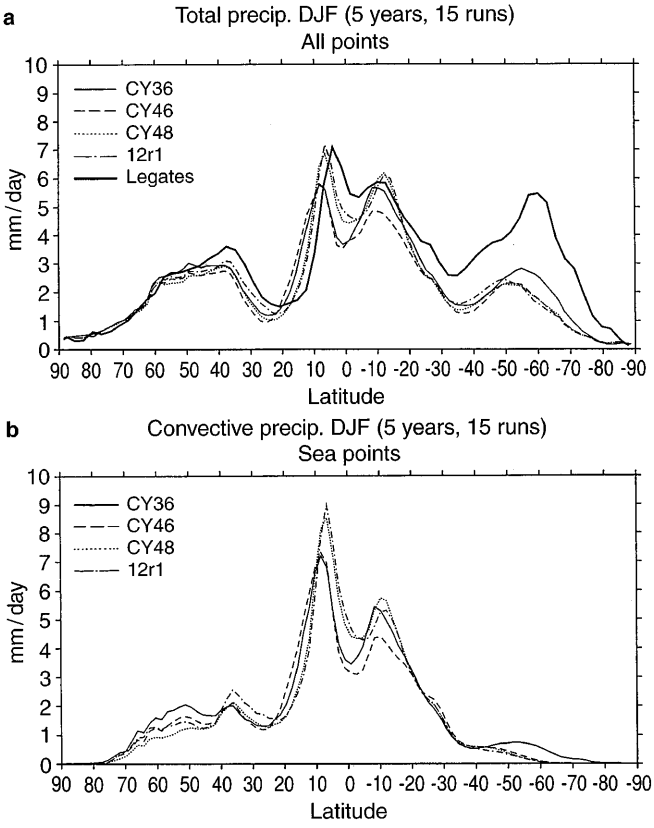

Fig. 11a, b. Zonally averaged ensemble mean DJF precipitation: **a** total over all points, **b** convective over sea points only. Units mmday^{-1}

is very similar in all four cycles (not shown). In both hemispheres between 50° and 60°, for example, CY36 convective precipitation is almost twice as large as CY48 (Fig. 10b). In the Southern Hemisphere storm track (around 60°S), the climate maximum greatly exceeds the model values. A similar result is found when the Jaeger (1976) climate is used as the reference, in spite the fact that the latter is systematically drier than the Legates and Willmott (1990) data. Even if the simulated Southern Hemisphere rainfall amounts are taken as a serious model deficiency, the discrepancy between the model and observed climatologies is so large that one may question the reliability of the observed climate data. Both rainfall climatologies are subject to high uncertainties in the Southern Hemisphere mid-latitudes because of large data void areas.

The global distribution of the DJF rainfall in the model cycles and for the DJF climate is shown in Fig. 12. The intensification of the Pacific ITCZ and SPCZ in CY48 and 12r1 relative to the other two cycles can be seen clearly. The Atlantic ITCZ off South America has intensified as well. The ITCZ double structure in the Indian Ocean which straddles the equator in CY46 becomes a broader structure with larger rainfall amounts in the later two cycles. The Australian rainfall is, apart from CY36, confined to the northern (monsoon rainfall) and eastern parts of the continent. This may be associated with the use of the new climatological albedo field which has a somewhat higher values over Australia in comparison to that used in CY36. Another marked change in the rainfall pattern is found over the Amazon basin immediately to the south of the equator. Both CY48 and 12r1 exhibit there much reduced rainfall amounts compared with CY46. In contrast, over southern Africa they produce more rain than CY46.

In the extratropics, differences between the model cycles are relatively small, both in amplitude and spatial coverage. Along the Northern storm tracks, somewhat less rain is found in CY48 than in the other three cycles. In the Southern Hemisphere storm track, CY36 has more rain than the other cycles (see Fig. 11).

The main differences between model and climate (Fig. 12e) precipitation fields may be summarized as follows. In the model, regardless of the cycle, the Pacific ITCZ is represented by a relatively narrow band of rainfall and elongated maximum, while in the climate the ITCZ is wider with a well-defined rainfall maximum at about 140°W. However, an elongated ITCZ rainfall maximum in observed data, similar to that seen in the model but with a weaker amplitude, is found by Dorman and Bourke (1979).

The climatological Indonesian maximum is much higher than any of the simulated ones; in the model it is characterized by "spotty" maxima scattered over Indonesian and Philippine islands with (too low) rainfall minima between them. It could be said that the simulated rainfall pattern over this region is dominated by orographic features. The influence of orography is even more pronounced in the model rainfall amplitude and pattern over Central and South America. The In-

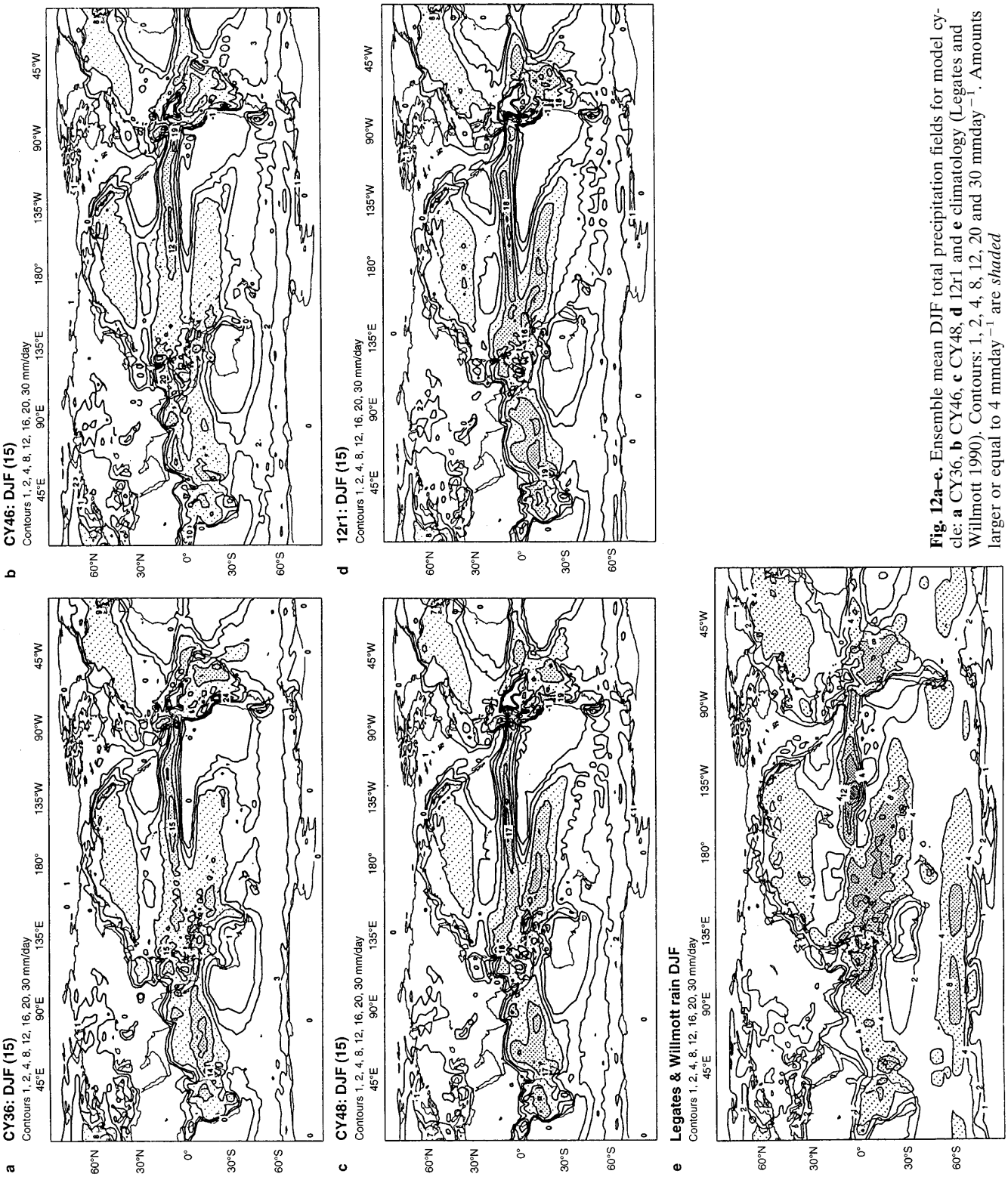

Fig. 12a–e. Ensemble mean DJF total precipitation fields for model cycle: **a** CY36, **b** CY46, **c** CY48, **d** 12r1 and **e** climatology (Legates and Willmott 1990). Contours: 1, 2, 4, 8, 12, 20 and 30 mmday^{-1}. Amounts larger or equal to 4 mmday^{-1} are *shaded*

dian Ocean ITCZ in the model is more intense than that in the climate data. In the extratropics, the climate has somewhat more rainfall than the model in both Northern storm tracks; in the Southern Hemisphere the modelled precipitation rate is very much underestimated (see also discussion earlier).

7 Simulation of interannual variability

7.1 Differences between two strong ENSO winters

The impact of different model formulations on simulation of interannual variability is discussed first in terms

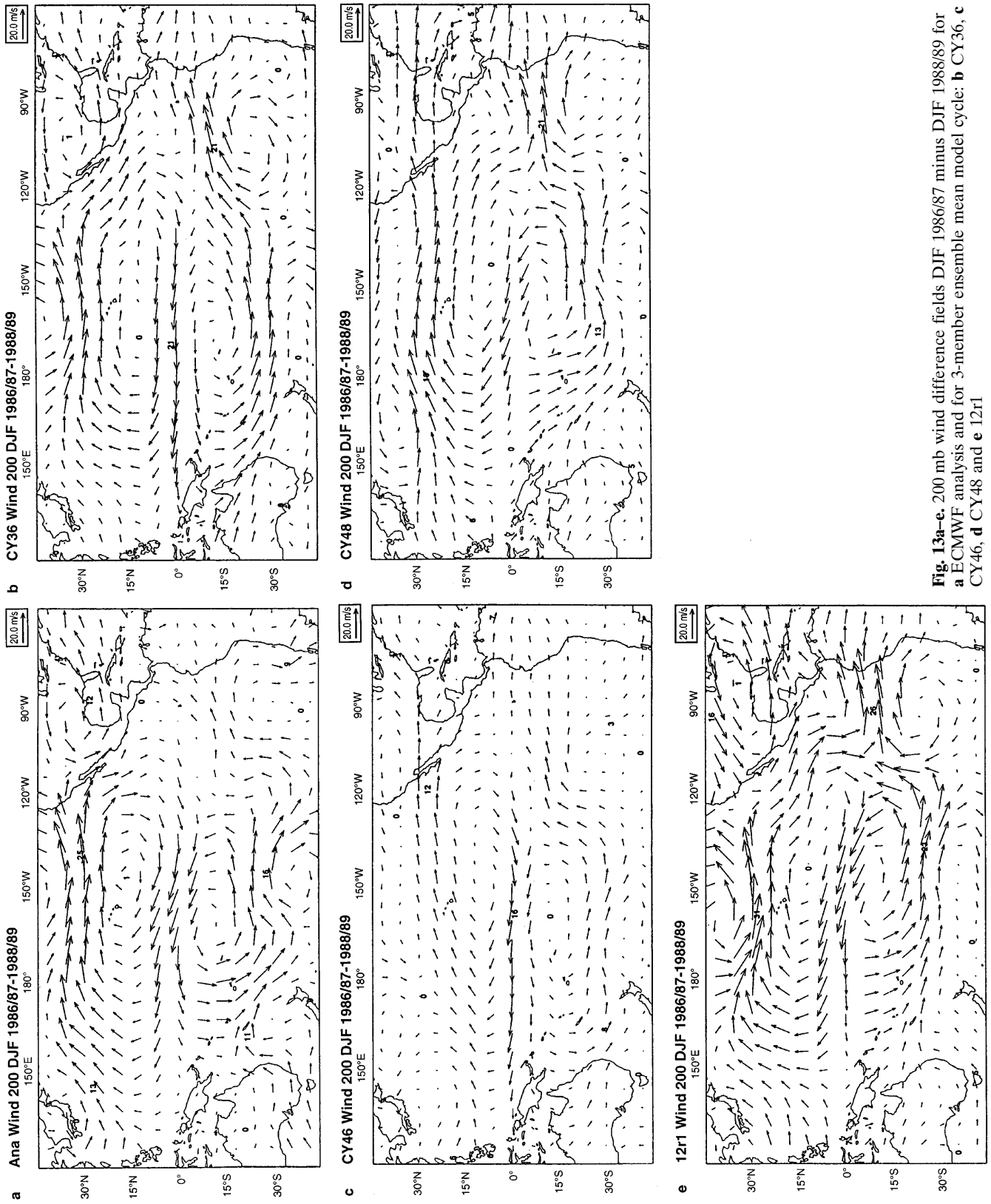

Fig. 13a–e. 200 mb wind difference fields DJF 1986/87 minus DJF 1988/89 for **a** ECMWF analysis and for 3-member ensemble mean model cycle: **b** CY36, **c** CY46, **d** CY48 and **e** 12r1

of the modelled differences between two strong ENSO index winters, DJF 1986/87 and DJF 1988/89. The former was an El Niño year with a strong positive SST anomaly in the equatorial Pacific; the latter was a La Niña year with a strong negative Pacific SST anomaly (see Branković et al. 1994, for a description of the SST anomalies in the period 1986 to 1990).

The two strong ENSO events and six model realizations may seem inadequate to come to a conclusion on statistical significance of the model response to tropical

SST forcing; a particular ENSO event can be very different from some canonical composite cases. Nevertheless, this "case study" is a good test of the model's ability to simulate these extreme climate events. The different solutions within the model ensembles could provide a measure of uncertainty associated with the internal variability of the atmosphere, since the "observed solution" is just one of many realizations under the same forcing conditions. Although figures will not be shown for brevity, the average model response discussed was found to be significant when differences between individual ensemble members were considered (see, e.g., Branković and Palmer 1996).

Tropical Pacific. The response of the 200 mb vector wind to the interannual differences in SST forcing in the tropical Pacific is presented in Fig. 13. In the analysis (Fig. 13a), the central Pacific wind differences resemble the flow anomaly obtained in the Gill (1980) linear model when forced with a low-level equatorial heating. On either side of the equator a pair of closed anticyclonic circulations is clearly seen, associated with relatively strong easterlies along the equator. The large magnitude of the Pacific differential circulation in Fig. 13a reflects the differences in the two anomaly fields driven by a relative strong SST forcing of the opposite sign. The cyclonic curvature further north in the Northern Pacific is indicative of negative geopotential differences, part of a broader PNA teleconnection wave train pattern.

In the model ensemble averages, both the shape and intensity of the Pacific differential circulation are captured reasonably well with all cycles except CY46, indicating a correct model response to the low-level heating anomalies. This circulation is very much underestimated in CY46. Both CY48 and 12r1 produce realistic equatorial easterlies and differential circulation south of the equator. CY36 produces more realistic differences in the northern subtropical Pacific, particularly southerly wind differences between 150°E and 180° and a cyclonic curvature along 30°N. In all cycles apart from CY46, the westerly differential flow off the South America western coast is overestimated, and extends too far across the South American continent into the Atlantic.

At 850 mb, over the tropical Pacific, the westerly differences are dominant, i.e. of the opposite sign to those aloft (not shown). This feature is well represented in the model, but with too strong a magnitude, especially in CY36. This may be interpreted as the tendency of the model to enhance the 850 mb divergence (or reduce convergence) in the western Pacific. The weakest wind differences are again found in CY46.

Northern extratropics. The response of the northern extratropical atmosphere to the strong differences in the equatorial Pacific SST forcing in winters of 1986/87 and 1988/89 is discussed in terms of 500 mb height differences (Fig. 14). In the analysis (Fig. 14e), the wave train structure extends from the tropical Pacific, over North America, into the tropical Atlantic. Such a wave train is typical of a positive PNA teleconnection pattern as described in, for example, Horel and Wallace (1981). In addition, two further centres are seen: positive in the north Atlantic, between Greenland and Iceland, and negative over Europe. Similar to the wind field, the height differences are of much larger amplitude than in standard anomaly fields for individual seasons (see Fig. 15a).

The model simulated, ensemble mean height differences between the two winters are shown in Fig. 14a–d. Apart from CY46, a well-established wave train over the PNA region, similar to that in the analysis, is seen for the other model cycles. The North American maximum and the adjacent oceanic minima are well located in CY36 and 12r1 when compared with the analysis, but displaced westward in CY48. On the other hand, CY48 as well as 12r1 represent well the negative differences over Europe, which are underestimated in CY36. In CY36 and CY48, amplitudes of differences over the PNA region are somewhat weaker than the analyzed ones, while in 12r1 they are quite realistic. It has to be borne in mind that weaker amplitudes in an ensemble mean may reflect the smoothing due to averaging of three model realizations for a relatively chaotic extratropical atmosphere.

The CY46 representation of interannual variation for 500 mb heights is very poor (Fig. 14b). The amplitude of differences is much smaller than in the other three model cycles. A major deficiency is the almost complete absence of the north Pacific minimum. The North American maximum is also much weaker and confined to the Alaskan region; thus no characteristic PNA wave train pattern in CY46 can be seen.

Another way to assess the ability of the model to represent interannual variability is to compare the difference in the frequency of atmospheric large-scale regimes between the El Niño and the La Niña winters. For this purpose, the five planetary wave clusters discussed in Sect. 5.2 have been used. Although sampling problems certainly affect individual winter estimates, the predominance of the positive-PNA clusters (1 and 2) in 1986/87 and of negative-PNA clusters (3 and 5) in 1988/89 was simulated in all model cycles except CY46, with 12r1 having the best agreement with observations (not shown). This is consistent with well-documented relationships between SST and extratropical flow anomalies.

7.2 Model errors in two strong ENSO winters

In this subsection we investigate the relationship between model simulated interannual variability for seasons DJF 1986/87 and DJF 1988/89, discussed already, and model mean errors. This is carried out for CY36, CY48 and 12r1, because, as inferred from Fig. 14, these model versions give better representation of Northern Hemisphere interannual variation than CY46. Ideally, the model error in each year representing strong interannual variation should be small, and the systematic error pattern should be insensitive to the observed anomaly.

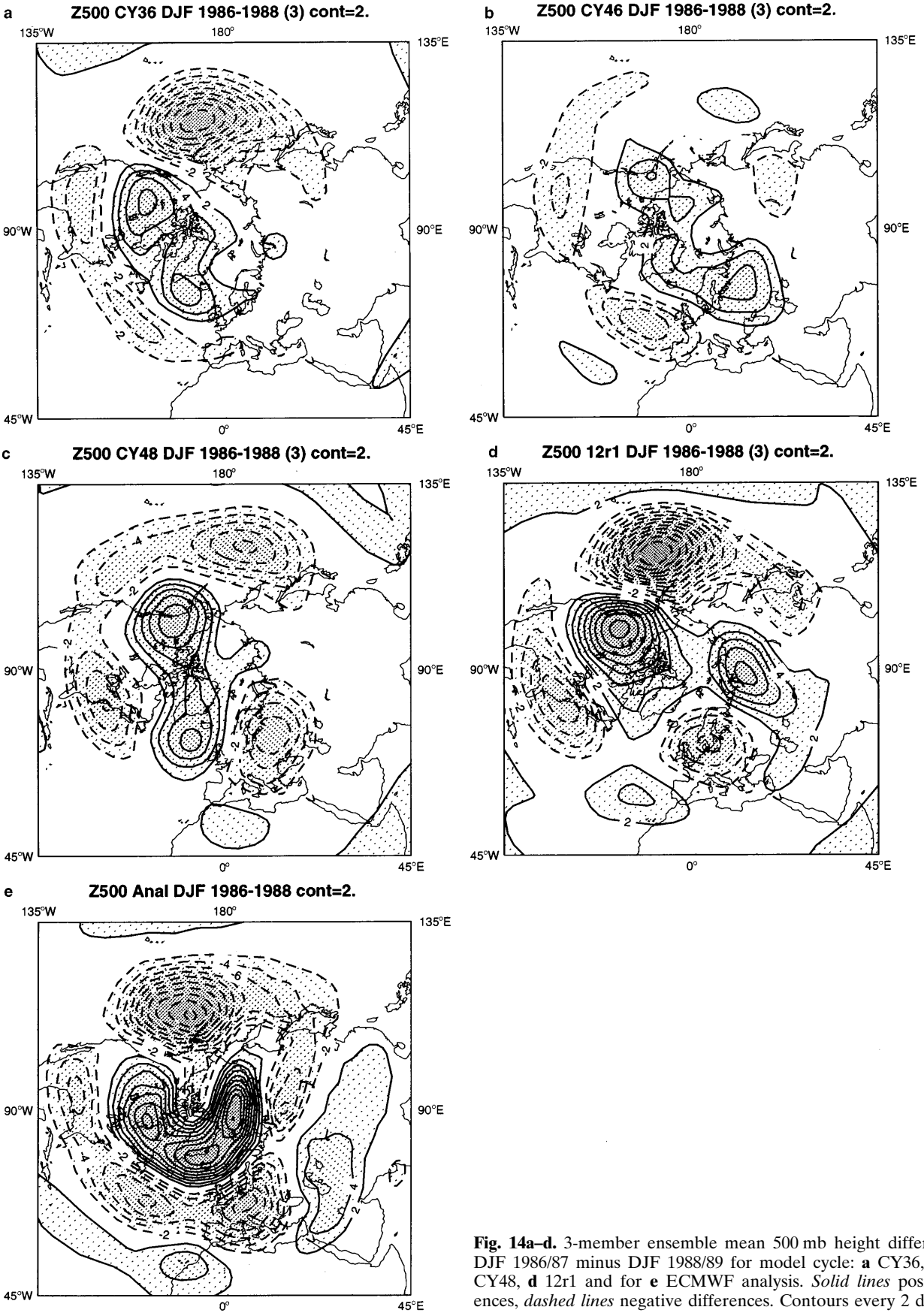

Fig. 14a–d. 3-member ensemble mean 500 mb height difference fields DJF 1986/87 minus DJF 1988/89 for model cycle: **a** CY36, **b** CY46, **c** CY48, **d** 12r1 and for **e** ECMWF analysis. *Solid lines* positive differences, *dashed lines* negative differences. Contours every 2 dam

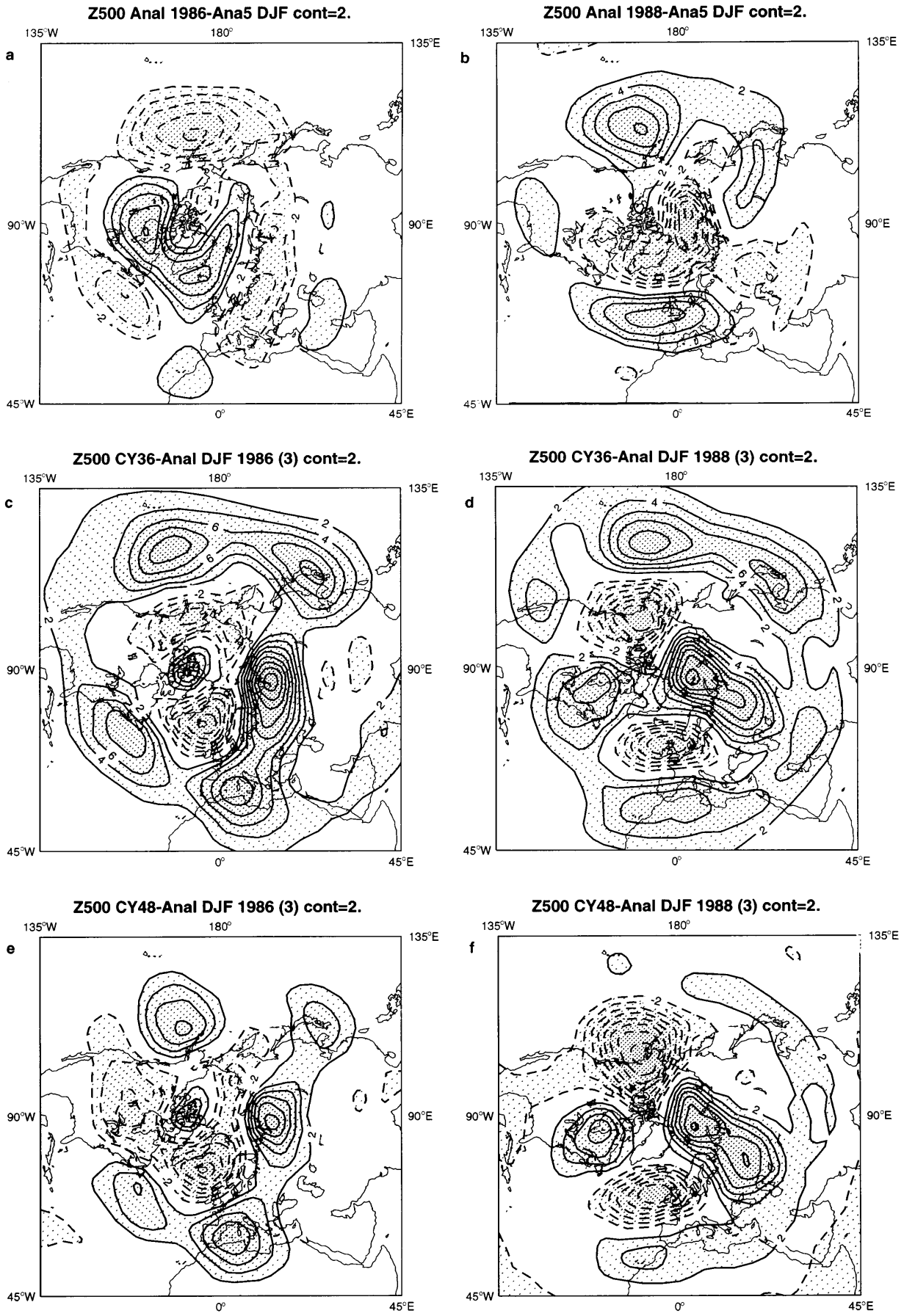

Fig. 15a–h. DJF 500 mb height analysis anomaly for **a** 1986/87, **b** 1988/89; 3-member ensemble mean DJF 500 mb height error for **c** CY36 1986/87, **d** CY36 1988/89, **e** CY48 1986/87, **f** CY48 1988/89, **g** 12r1 1986/87 and **h** 12r1 1988/89. *Solid lines* positive anomalies/errors, *dashed lines* negative anomalies/errors. Contours every 2 dam

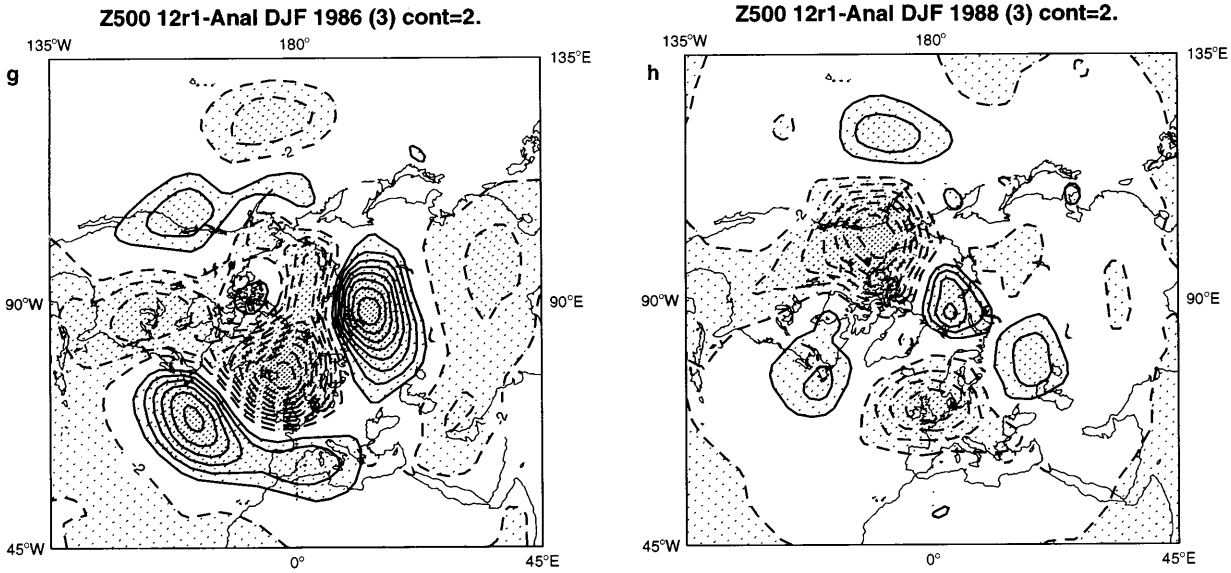

Fig. 15. (Continued)

Figure 15a, b shows analyzed 500 mb height anomalies for DJF 1986/87 and DJF 1988/89 respectively. The relatively large amplitudes and the opposite sign of anomalies over the PNA and Atlantic/European regions are typical of a mid-latitude atmospheric response to a strong and opposite equatorial Pacific SST anomaly forcing.

CY36 ensemble mean errors in both winters are very similar (Fig. 15c, d). Despite some differences in the amplitude of errors, the basic error pattern is common to both winters: a positive error over the northern Pacific, a negative error over the Alaskan region and positive again over the eastern coast of North America. In the La Niña winter (Fig. 15d), due to a stronger negative error over Alaska, the Atlantic/European error dipole is shifted southeastward. The occurrence of large and similar errors in these two winters, despite different SST anomaly boundary forcing, is indicative of a strong systematic bias in CY36 (see also the t-statistic in Fig. 1a).

On the other hand, the CY48 errors (Fig. 15e, f) over the PNA region in DJF 1986/87 are different from those in DJF 1988/89. Positive error over the north Pacific in the El Niño winter (where the analysis anomaly is negative) is replaced with a relative strong negative error in the La Niña winter (when the analysis anomaly is positive). Again, over the eastern part of North America errors in these two winters are of the opposite sign (and opposite to the analysis anomalies). Overall, the mean error pattern in CY48 behaves less systematically in comparison with CY36. The fact that CY48 errors over much of the Northern Hemisphere are almost opposite to observed anomalies would imply that CY48 tends to underestimate the response to SST anomalies.

Though cycle 12r1 errors (Fig. 15g, h) may appear similar to those of CY48, the main differences are the following. The 12r1 error amplitudes are larger than in CY48 over the Atlantic/European and Asian regions in the El Niño winter and smaller (over the same regions) in the La Niña winter. A detailed inspection of Fig. 15g, h indicates a slight eastward shift in the positioning of the PNA error centres in 12r1 relative to CY48. The reduced systematic error of 12r1 in the Pacific region, shown in Fig. 2d, seems to have played an important role in a relatively successful representation of interannual variability by this model cycle, as shown in Fig. 14d.

This discussion is further supported by the 500 mb height correlation coefficients between analyzed anomalies and model errors for the two winters. These are shown in Table 2 for the PNA and Atlantic/European regions. (The regions' boundaries are identical to those defined in Branković et al. 1994.) If the model error pattern was identical to the analysis anomaly pattern but of the opposite sign, the correlation coefficient would be exactly −1. Table 2 shows that in both winters, CY48 has the strongest tendency to counteract analyzed anomalies, consistent with the discussion earlier. 12r1 seems to be superior to CY36 because, on average, it has weaker correlations than CY36.

8 Summary and conclusions

Four different versions (cycles) of the ECMWF NWP model have been integrated at low (T63) resolution on

Table 2. The 500 mb height correlation coefficients between analysis anomalies and model ensemble mean errors for El Niño and La Niña winters

	DJF 1986/87		DJF 1988/89	
	PNA	Atlantic/Europe	PNA	Atlantic/Europe
CY36	−0.45	−0.67	0.02	−0.48
CY48	−0.68	−0.80	−0.60	−0.56
12r1	−0.15	−0.66	−0.18	−0.35

the seasonal time scale in order to study the influence of various model formulations on model climate. The model versions, denoted as cycles 36, 46, 48 and 12r1, differ primarily in the representation of physical processes, but in cycle 12r1 a higher vertical resolution was also used for technical reasons (however, without changing the model vertical domain). The successive cycles were introduced in ECMWF operations over the period of about four years, from 1990 to 1994.

For five northern winter seasons (DJF 1986/87 to 1990/91) three 120-day experiments, initiated from initial data one day apart, were run for each model cycle. The four model climatologies were derived as averages of 15 integrations in each cycle. In the first three cycles the observed SST was updated every five days throughout the experiment integration, but was updated daily in cycle 12r1.

With the introduction of cycle 48, an apparent improvement in the Northern Hemisphere wintertime climate of ECMWF model has been observed. A strong systematic bias in the earlier cycles in the Northern Hemisphere, associated with an overestimation of the zonal flow in the eastern Pacific and a weak diffluence over western North America, was reduced and replaced by more realistic ridging over the north Pacific/Alaskan region. This error has been further reduced in cycle 12r1. The improvement is associated with a reduction in the temperature error over the northeastern Pacific. A reduction of errors in zonally averaged zonal wind and eddy kinetic energy is also evident.

While cycle 46 exhibits reduced model errors in the Southern Hemisphere summer, its contribution to the Northern Hemisphere winter mean flow is not evident. It was argued that the impact of the revised cloud shortwave optical properties introduced with cycle 46 is strongly susceptible to seasonal forcing. However, other model changes introduced between cycle 36 and cycle 46 may also have contributed to the reduction of the Southern Hemisphere errors.

The frequency of blocking with cycle 12r1 is much more realistic over the north Pacific region when compared with the other three cycles, though it was slightly improved already in cycle 48. It was argued that this improved representation of the northern Pacific block is due to more efficient diabatic response to the warm SSTs over the western equatorial Pacific. A slight deterioration of blocking frequency in cycle 12r1 over the Atlantic/European region is associated with the strengthening of the Atlantic jet in comparison with the other cycles.

Different possible mechanisms may be considered to be the cause of an increase in the frequency of blocking events over the north Pacific region with cycle 12r1. Hoerling and Ting (1994) discussed the relative importance of tropical Pacific diabatic heating and extratropical transient forcing in the maintaining the extratropical wave train over the PNA region. Here, the main contribution to the anomalous transient forcing comes from high frequency baroclinic waves associated with the North Pacific storm track. According to Fig. 5, the North Pacific high-frequency variability in cycle 12r1 is somewhat weakened in comparison with other model cycles. On the basis of these simple arguments, it seems feasible to ascribe an improved frequency of Pacific blocks in cycle 12r1 to (a more efficient) tropical forcing. However, a more detailed diagnostics is required to fully substantiate or otherwise such a hypothesis.

Not all parameters exhibited an improvement in the climate drift in successive cycles. For example, in the lower troposphere a negative temperature error has slightly increased over the oceans from cycle 46 to cycle 48. This is associated with an increase in the lower tropospheric humidity in cycle 48 relative to cycle 46. There was a small increase in the height of the PBL in cycle 48 due to the introduction of entrainment at the top of the PBL. Such an increase causes, on average, the 850 mb level to occur more often in or below the PBL inversion and therefore temperature at 850 mb decreases and moisture increases. The effect of the entrainment in shallow convection also contributes to the moistening around 850 mb level.

A relative warming over the tropical continents, on the other hand, implies further drying and larger errors in cycles 48 and 12r1. A strong polar stratospheric cooling in both hemispheres is still seen in cycle 12r1, however, this has been greatly reduced in the Southern (summer) Hemisphere. A warming of the tropical lower stratosphere, which became apparent with the introduction of cycle 46, is still very much evident in cycle 12r1. This error is not unique to seasonal integrations, it has been also seen in the ECMWF operational medium-range forecasts.

The Hadley circulation, which was somewhat weakened from cycle 36 to cycle 46, has become more intense again with the later cycles. The lower branch of the large-scale tropical ascent is now overestimated when compared with the operational analysis (which, however, is likely to be deficient in this respect). This is associated with an intensification in convective rainfall within the tropical convergence zones in cycles 48 and 12r1, particularly over the Pacific, and to a more active shallow convection in these cycles. Another prominent feature of the later cycles is the concentration of tropical precipitation into relatively narrow bands that represent the main tropical convergence zones. Lack of observations to provide climatological data makes the verification of the Southern Hemisphere model precipitation uncertain.

In terms of representing the Northern Hemisphere circulation, model cycles 36 and 46 are comparable and cycles 48 and 12r1 can be regarded as improvements over the former two cycles. Cycle 36 has a relatively strong systematic bias which is insensitive to analysis anomalies in winters of 1986/87 and 1988/89. In simulating interannual variability for the two strong and opposite ENSO-index winters, cycle 46 is the least successful. This interannual variation seems to be most realistically represented with cycle 12r1. The relatively small mean errors in cycle 48 are explained by a partial offset between model errors in strong and opposite ENSO years. Such a model behaviour requires a cau-

tious interpretation of the model representation of interannual variation in the presence of strong and opposite SST forcings (see also Mo and Wang 1995).

Verifications of modelled low-frequency variability in terms of frequency of the Northern Hemisphere flow regimes indicate a reasonable similarity between analyzed and modelled frequencies for all cycles when results from the whole set of experiments are compared with the 5-year and 12-year analysis data. The interannual variability of cluster frequencies between opposite ENSO phases is reproduced most satisfactorily by cycle 12r1.

Overall, the most recent ECMWF model versions, cycle 48 and especially cycle 12r1, have generally a better wintertime climatology than earlier versions. On seasonal time scales, some of the model systematic errors have been steadily reduced and the model's ability to reproduce interannual variations has been improved. Consistently with the results of other studies (e.g. Miyakoda et al. 1983; Sirutis and Miyakoda 1990; Hurrell 1995), we have shown that the development of more sophisticated physical parametrizations led to substantial improvements in the ECMWF model climate. However, despite such improvements the process of diagnosing and correcting deficiencies in the ECMWF model climate still requires considerable effort and seasonal integrations have proved to be a valuable complement to the diagnostics of operational forecasts.

Acknowledgements. We thank Mike Blackburn, Tony Hollingsworth, Martin Miller, Jean-Jacques Morcrette, Tim Palmer and Adrian Simmons for constructive discussions and valuable comments on earlier version of the paper. We also appreciate comments and suggestions by two reviewers, David Stephenson and an anonymous reviewer, that greatly improved the paper.

References

Beljaars ACM (1995) The parametrization of surface fluxes in large-scale models under free convection. Q J R Meteorol Soc 121:255–270

Beljaars ACM, Viterbo P, Miller MJ, Betts AK (1996) The anomalous rainfall of the United States during July 1993: sensitivity to land surface parametrization and soil moisture anomalies. Mon Weather Rev 124:362–383

Boer GJ, Arpe K, Blackburn M, Déqué M, Gates WL, Hart TL, Le Treut H, Rockner E, Sheinin DA, Simmonds I, Smith RNB, Tokioka T, Wetherald RT, Williamson D (1991) An intercomparison of the climates simulated by 14 atmospheric general circulation models. CAS/JSC Working Group on Numerical Experimentation, Rep 15, WMO/TD-No. 425

Branković Č, Ferranti L (1992) Seasonal integrations with realistic boundary forcing. Proceedings of the ECMWF Workshop "New Developments in Predictability". ECMWF, Shinfield Park, Reading, UK, 13–15 November 1991, 305–333

Branković Č, Palmer TN (1996) Atmospheric seasonal predictability and estimates of ensemble size. Mon Weather Rev (in press)

Branković Č, Palmer TN, Ferranti L (1994) Predictability of seasonal atmospheric variations. J Clim 7:217–237

Dorman CE, Bourke RH (1979) Precipitation over the Pacific Ocean, 30°S to 60°N. Mon Weather Rev 107:896–910

Ferranti L, Molteni F, Branković Č, Palmer TN (1994a) Diagnosis of extra-tropical variability in seasonal integrations of the ECMWF model. J Clim 7:849–868

Ferranti L, Molteni F, Palmer TN (1994b) Impact of localized tropical and extratropical SST anomalies in ensembles of seasonal GCM integrations. Q J R Meteorol Soc 120:1613–1645

Gill AE (1980) Some simple solutions for heat-induced tropical circulations. Q J R Meteorol Soc 106:447–462

Hoerling MP, Ting M (1994) Organization of extratropical transients during El Niño. J Clim 7:745–766

Horel JD, Wallace JM (1981) Planetary-scale atmospheric phenomena associated with southern oscillation. Mon Weather Rev 109:813–829

Hurrell JW (1995) Comparison of NCAR Community Climate Model (CCM) climates. Clim Dyn 11:25–50

Jaeger L (1976) Monatskarten des Niederschlags für die ganze Erde. Ber Dtsch Wetterdienstes 139:Band 18

Kaas E, Branstator G (1993) The relationship between a zonal index and blocking activity. J Atmos Sci 50:3061–3077

Lary DJ, Balluch M (1993) Solar heating rates: the importance of spherical geometry. J Atmos Sci 50:3983–3993

Legates DR, Willmott CJ (1990) Mean seasonal and spatial variability in gauge-corrected, global precipitation. Int J Climatol 10:111–127

Le Treut H (ed) (1996) Climate sensitivity to radiative perturbation: Physical mechanisms and their validation. NATO ASI Series, Springer, Berlin Heidelberg New York

Miller MJ, Beljaars ACM, Palmer TN (1992) The sensitivity of the ECMWF model to parametrization of evaporation from the tropical oceans. J Clim 5:418–434

Miyakoda K, Sirutis J (1990) Subgrid scale physics in 1-month forecasts. Part II: systematic error and blocking forecasts. Mon Weather Rev 118:1065–1081

Miyakoda K, Gordon T, Caverly R, Stern W, Sirutis J (1983) Simulation of blocking event in January 1977. Mon Weather Rev 111:846–869

Mo KC, Wang XL (1995) Sensitivity of systematic error of extended range forecasts to sea surface temperature anomalies. J Clim 8:1533–1543

Molteni F, Tibaldi S, Palmer TN (1990) Regimes in the wintertime circulation over northern extratropics. I: observational evidence. Q J R Meteorol Soc 116:31–67

Morcrette J-J (1993) Revision of the clear-sky and cloud radiative properties in the ECMWF model. ECMWF Newsl 61:3–14

Mullen SL (1989) Model experiments on the impact of Pacific sea surface temperature anomalies on blocking frequency. J Clim 2:997–1013

Palmer TN, Branković Č, Molteni F, Tibaldi S (1990) Extended-range predictions with ECMWF models: Interannual variability in operational model integrations. Q J R Meteorol Soc 116:799–834

Sirutis J, Miyakoda K (1990) Subgrid scale physics in 1-month forecasts. Part I: experiment with four parametrization packages. Mon Weather Rev 118:1043–1064

Slingo JM, Sperber KR, Boyle JS, Ceron J-P, Dix M, Dugas B, Ebisuzaki W, Fyfe J, Gregory D, Gueremy J-F, Hack J, Harzallah A, Inness P, Kitoh A, Lau WK-M, McAvaney B, Madden R, Matthews A, Palmer TN, Park C-K, Randall D, Renno N (1996) Intraseasonal oscillations in 15 atmospheric general circulation models: results from an AMIP diagnostic subproject. Clim Dyn 12:325–357

Tibaldi S, Molteni F (1990) On the operational predictability of blocking. Tellus 42A:343–365

Viterbo P, Beljaars ACM (1995) An improved land surface parametrization scheme in the ECMWF model and its validation. J Clim 8:2716–2748

WMO, CAS/JSC Working group on numerical experimentation (1988) Workshop on systematic errors in models of the atmosphere. Toronto, Canada, 19–23 September 1988. WMO/TD-No. 273

WMO, PLRF (1991) ICTP/WMO Technical conference on long-range weather forecasting research. Trieste, Italy, 8–12 April 1991, WMO/TD-No. 395